CHAPTER 4

Novel triphenylene-based ionic discotic liquid crystals

4.1 Introduction

Ionic liquid crystals are a class of compounds that contains anions and cations. Ionic liquid crystals can be considered as materials that combine the properties of liquid crystals and ionic liquid. The ionic character means that some of the properties of the ionic liquid crystal differ significantly from that of conventional liquid crystals. Typical for ionic liquid crystals is the ion conductivity. The ionic interactions tend to stabilize lamellar mesophases, but ionic liquid crystals also display uncommon mesophases such as nematic columnar phase [1].

At present, worldwide intense research activity in the field of ionic liquids is going on [2-9]. The main driving force to explore ionic liquids is the fact that these compounds have a very low vapor pressure, so that they are candidates to replace volatile organic solvents in organic reactions. The properties of ionic liquids mainly, miscibility with water and other solvents, dissolving ability, polarity, viscosity, density can be tuned by an appropriate choice of the anion and the cation and that's why ionic liquids are often considered as designer solvents. These ionic liquids can also be used to immobilize transition metal catalysts in the liquid phase of biphasic catalytic reactions. Additionally, it is well known that ionic molecules form amphotropic liquid crystals (LCs) [10]. They have great potential as ordered reaction media that can impart selectivity in reactions by ordering reactants [11]. The formation of supramolecular assemblies containing ionic liquids may find applications as heat carriers in solar-thermal energy generators and as electrolytes for batteries and capacitors [12].

Alkali metal soaps were the first salts identified as displaying liquid crystalline properties, followed by alkylammonium, pyridinium, vinamidinium, phosphonium, imidazolium salts, etc [13-25]. A number of calamitic liquid crystalline imidazolium salts have recently been prepared and the formation of lamellar phases in these materials has been recognized [18, 20, 26, 27]. Self-assembly of a non-liquid crystalline imidazolium ionic liquid and a hydroxyl-terminated liquid crystal leads to the formation of phase-segregated layered structures on the nano scale. These materials have been found two-dimensional ionic conductivities with high anisotropy [28]. Similarly a two-dimensional ion-conductive material formed by self-organization of dihydroxy-functional rod-like molecules and ionic liquid has been reported in literature [29]. The chemistry of ionic liquid crystals has recently been covered in a review article by Binnemans [30].

4.2 Ionic discotic liquid crystals

Compare to the large number of calamitic ionic liquid crystals, discotic liquid crystalline ionic salts are rare. The Ringsdorf group [31] reported the synthesis of multipolar amphiphiles based on benzene & triphenylene as a discotic core with pyridinium or trimethylammonium head groups (**1**-**4**).

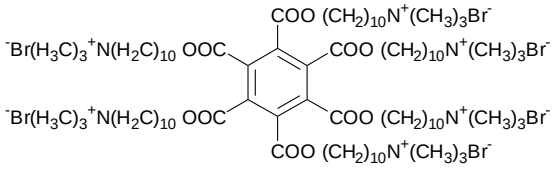

1

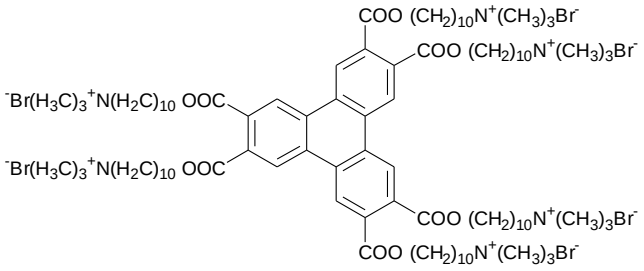

2

All these amphiphiles are very soluble in water. Interestingly, **1** and **3** are too soluble in water to form liquid crystals. On the other hand, triphenylene-based salt **2** shows a small hexagonal phase at room temperature and no liquid crystallinity at higher temperatures. The triphenylene derivative **4** with six decyl chains and pyridinium head groups forms a nematic phase of finite cylinders at concentrations below that of its hexagonal phase.

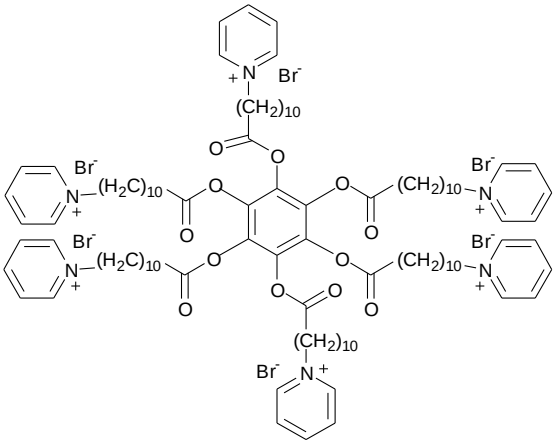

3

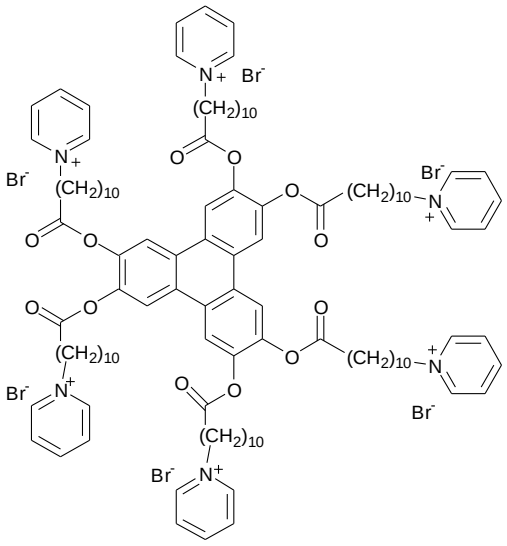

4

The highly unstable nature of a columnar phase forming a 2, 4, 6-triarylpyridinium salt (**5**) was mentioned by the Veber group [32].

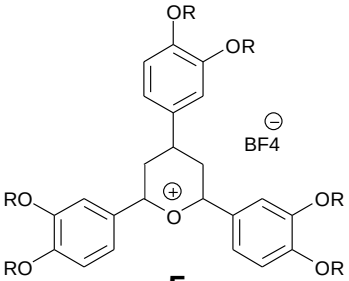

5

Amphotropic phthalocyanine **6** with liquid crystallinity has been reported by van Nostrun group [33]. This molecule was shown to adopt both perpendicular as well as parallel orientations on the water surface, depending on the applied surface pressure.

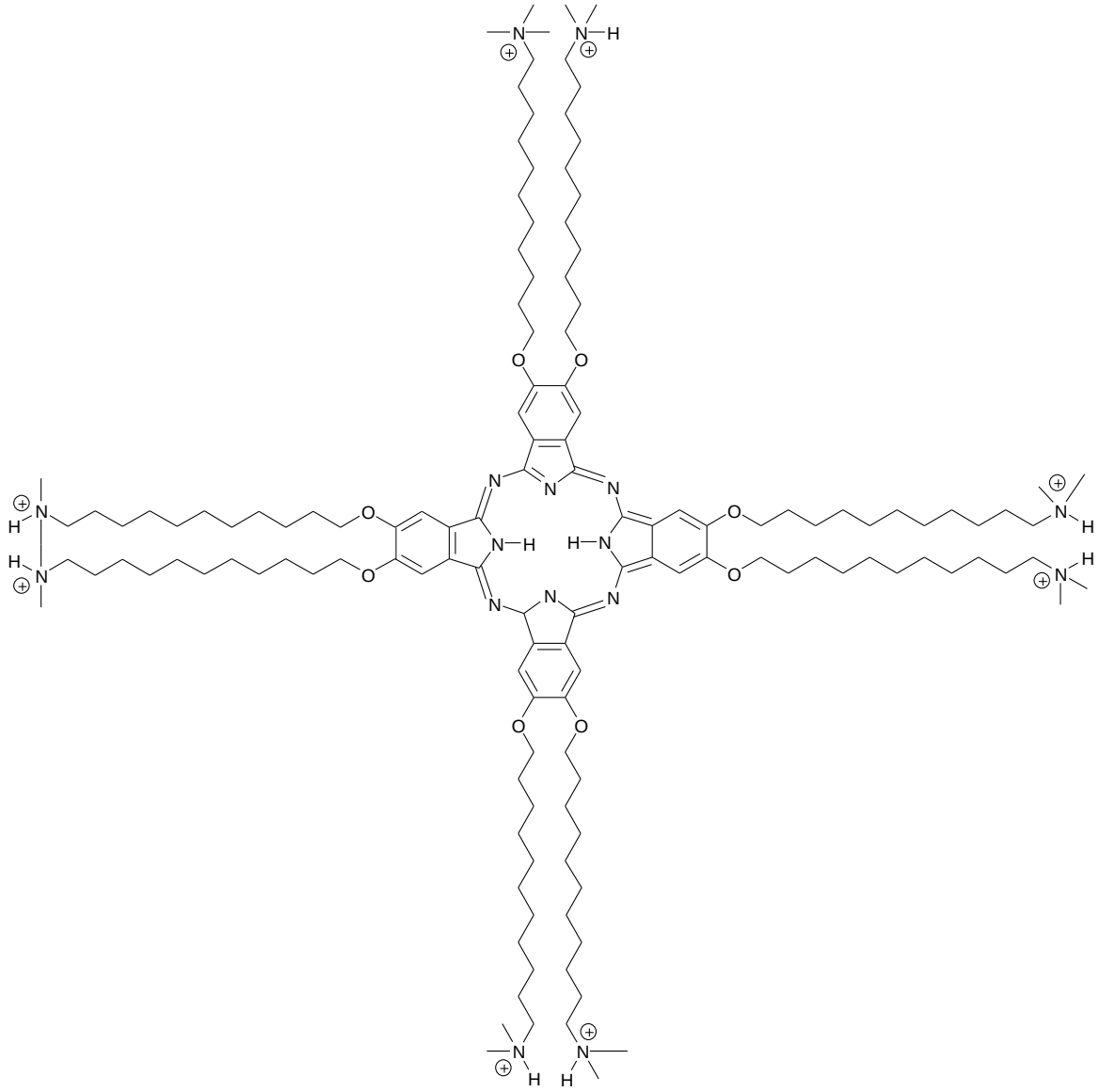

6

Discotic ionic molecules containing crown ethers are also known to show mesomorphism. For example, Percec *et al*. shows complexation of the crown ether receptor of the benzo-15-crown-5 benzoate **7** with $NaCF_3SO_3$ and KCF_3SO_3, which induces the self-assembly of a supramolecular cylindrical channel-like architecture displaying an enantiotropic thermotropic disordered hexagonal mesophase [34].

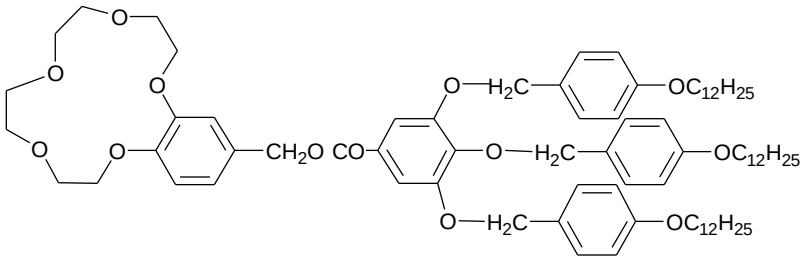

7

Beginn *et al*. reported [35] incorporation of functional channels based on the self-assembly of low-molecular weight amphiphile **8**, which enable supramolecular transport through the cylinders containing functionalized polymerizable olefin groups in the outer rim of the cylinder and functional receptor crown ether units in their center.

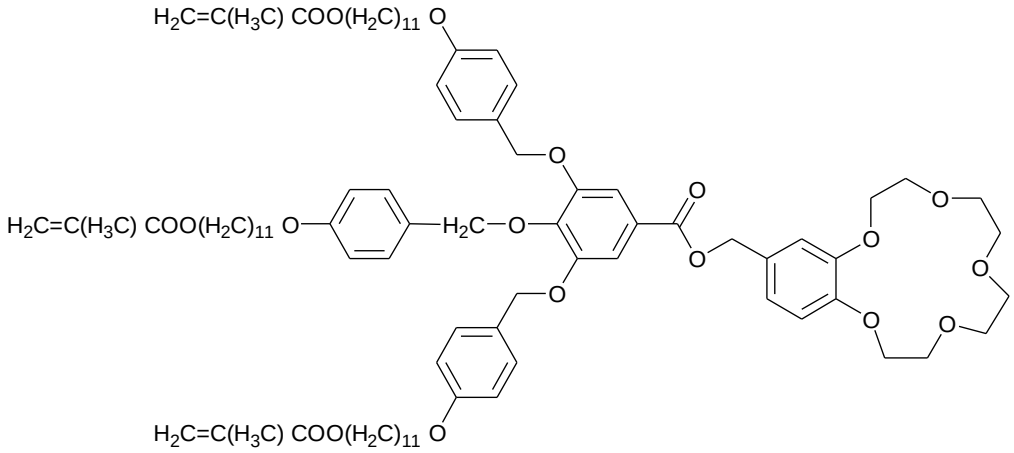

8

Yoshio *et al*. very recently reported the one-dimensional ion transport in self-organized columnar ionic liquids at the nanometer scale [36]. Despite the non-discotic shape (**9**) of the trialkoxybenzene substituted imidazolium salt, it forms a columnar phase in which the ionic conductivities parallel to the columnar axis were found to be higher than those perpendiculars to the axis [36].

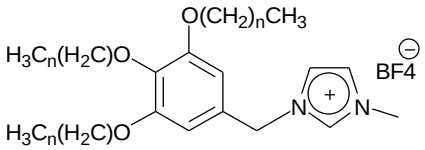

9a: n = 8

9b: n = 12

Discotic ionic liquid crystalline tricycloquinazoline (TCQ, **10**) has been used as a hexaionic building block for assembly into ordered liquid-crystalline aggregates using the ionic self-assembly technique [37].

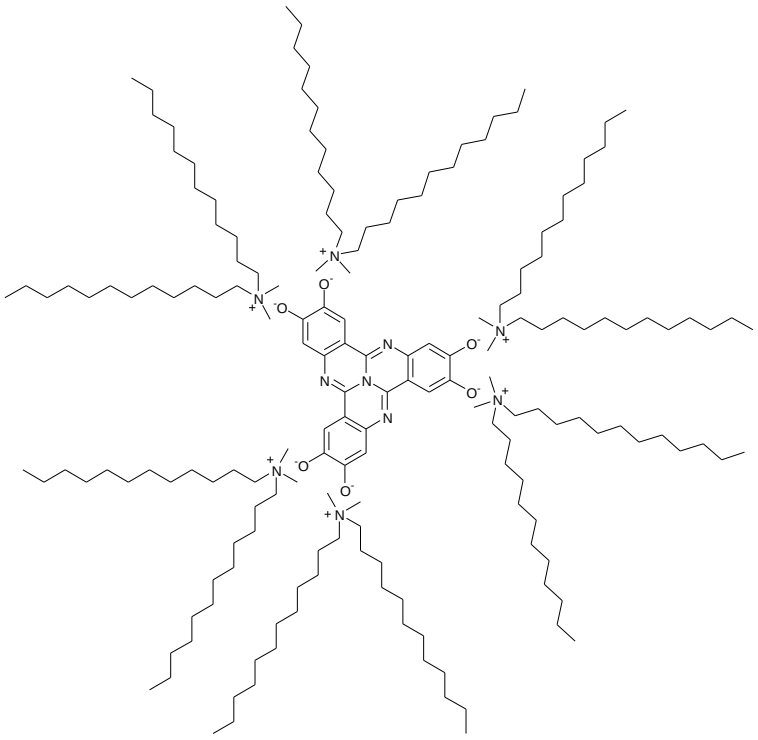

10

Kraft *et al*. reported [38] the self-assembly of long-chain alkoxy-substituted benzoic acids around tribasic core **11**, which provides a simple and flexible way to supramolecular liquid crystals with columnar mesophase through hydrogen bonding.

Recently, Motoyanagi *et al*. [39] showed that incorporation of imidazolium ion functionalities into paraffinic side-chain termini of a triphenylene derivative (**12**) resulted in stabilization of a columnar mesophase of its liquid crystalline assembly.

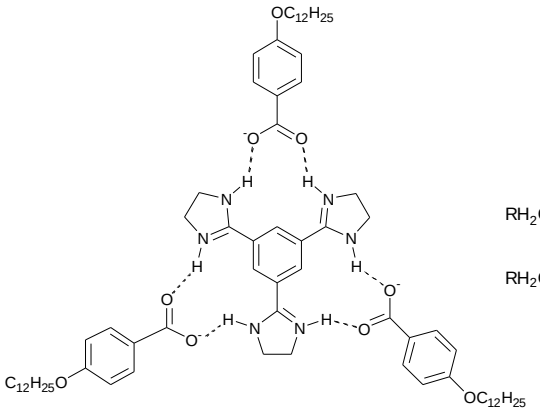

11

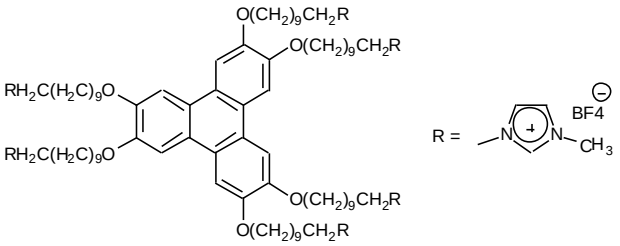

12

The compound **12** is very interesting as it retained columnar mesophase over a wide temperature range down to 4 °C in contrast to paraffinic triphenylene without imidazolium functionalities [40].

4.3 Objective

As mentioned in chapter 1, discotic liquid crystals [41] are renowned for their one-dimensional transportation of charge, ion and energy. For such functionalization, it is important to control orientation, supramolecular association, and phase segregation of the columnar assemblies from molecular to macroscopic scale [42]. Triphenylene derivatives are the archetypal discotic liquid crystals [43]. Columnar assembly of triphenylene derivatives can be used to prepare functional liquid crystalline electron-, ion-, or proton- conducting materials by using nano-segregation. The key to the success is in controlling the macroscale orientation of the conducting nanostructures.

On the other hand ionic liquids are functional isotropic liquids exhibiting high ionic conductivities. Recently, they are intensively investigated based on their remarkable properties such as chemical stability, incombustibility, non-volatility etc. They also have a possibility to be an ionic conducive material without mixing a salt as an alkali metal salt. Especially, the imidazolium and pyridinium salts are well known ionic liquids.

Hybridization of self-organizing triphenylene discotics with imidazolium and pyridinium ionic liquids may lead to novel materials with interesting properties that are useful for many device applications. With this in mind we have initiated this research program to incorporate imidazolium-based and pyridinium-based ionic liquids in the supramolecular order of discotic liquid crystals by attaching triphenylene discotics covalently to the imidazolium and pyridinium salts and study the effects of counter ions, spacers and peripheral substitution in these materials. The design strategy here is to modify ionic liquids to prepare simpler columnar assemblies that exhibit fluid ordered states, maintaining both of high ionic conductivities and liquid crystalline states at reasonable temperature ranges. In this chapter we describe the synthesis of novel pyridinium and imidazolium bromides containing hexaalkoxytriphenylene units and their thermotropic liquid crystalline properties.

4.4 Pyridinium-substituted triphenylene-based ionic liquid crystals

4.4.1 Synthesis

Compounds **17** were synthesized by the route shown in scheme 1. Hexalkoxytriphenylenes **14**, monohydroxytriphenylenes **15** and ω-bromo-substituted triphenylenes **16** were prepared following literature methods [44-46]. Thus oxidative trimerization of dialkoxybenzene **13** with $FeCl_3$ in presence of a catalytic amount of H_2SO_4 gives hexaalkoxytriphenylenes **14** in 65 % yield. Selective cleavage of one of the aryl-ether bond of **14** using B-bromocatecholborane furnished monohydroxytriphenylenes **15** in about 50 % yield. Monohydroxytriphenylene on reflux with appropriate dibromide in presence of Cs_2CO_3 as a base and ethyl methyl ketone as a solvent give rise to bromo-terminated triphenylene **16** in about 70 % yield. Pyridinium salts **17** were obtained by reacting the bromo-substituted compounds **16** with pyridine. Similarly, γ-

picoline was reacted with **16** to give substituted pyridinium salt **18**. Detailed synthetic procedure has been given in experimental section.

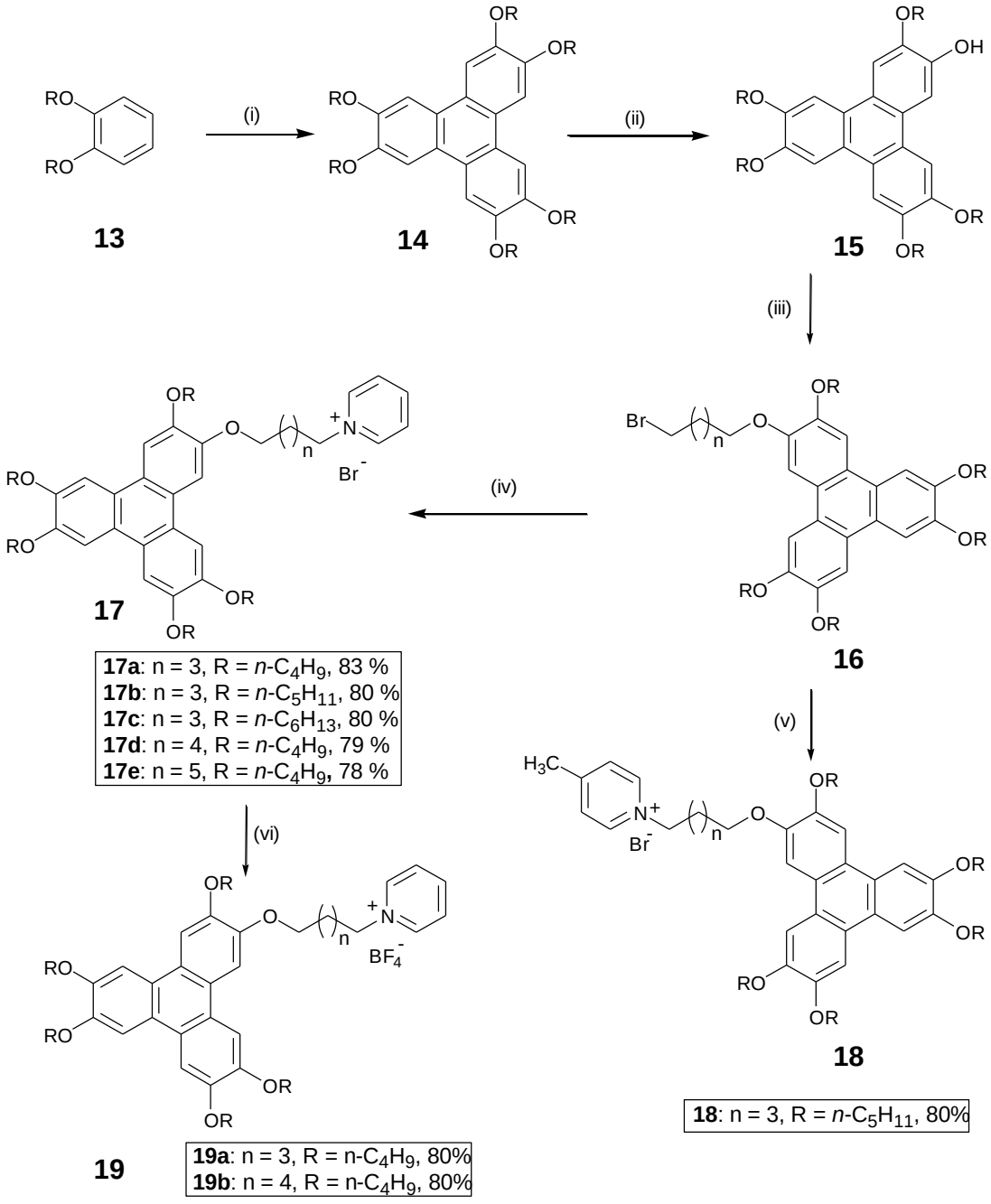

Scheme 1. Synthesis of triphenylene-substituted pyridinium salts. Reagents and conditions: (i), (ii), and (iii) as given in Ref. 70-73, (iv) pyridine, toluene, 80 °C, 8 hr, (v) γ-picoline, toluene, 80 °C, 8 hr, (vi) MeOH, $NaBF_4$, room temperature, 2 hr.

4.4.2 Characterization

All the compounds were purified by repeated column chromatography followed by crystallization and characterized from their ^{1}H NMR, ^{13}C NMR, IR, UV spectra and elemental analysis. All the members of the series give similar spectra. Spectral data and elemental analysis of all the compounds were in good agreement with their structures, indicating the high purity of all the materials.

Figure 1 represents the ^{1}H NMR spectrum of **17a**. There are four different types of aromatic protons which give rise to four signals at different δ values. As seen from the structure **17a**, protons which are ortho to nitrogen atom (H_b) are in the same environment and have the same δ values. These protons couple with the neighboring H_c protons and appear as doublet (d). As they are attached to aromatic ring having strongly electron withdrawing N atom they have δ values higher compare to other hydrogens (δ = 9.45, d, H_b protons). Having para to N atom, H_d proton resonates with lower δ value (δ = 8.3 ppm) compare to H_b protons and couples with neighbouring H_c protons to give a triplet in the NMR spectrum. Similarly H_c protons are in the same environment and will appear as a triplet (δ = 7.95 ppm) as a result of coupling between H_b and H_d atoms. All the six aromatic hydrogens of triphenylene moiety (H_a) appear as multiplets near δ value of 7.8 ppm. The $–OCH_2$ and $–N^+CH_2$ hydrogens give rise to multiplets (δ = 4.2 ppm) and triplets (δ = 5.1 ppm) respectively. Other aliphatic protons of the chains can be clearly seen in the spectrum. This confirms the structure and high purity of the compound. All other derivatives **17b-e**, **19a-b**, show similar spectrum differing only in the aliphatic protons. The ^{1}H NMR spectrum of compound **17b** and **17d** is reproduced in figure 2 and figure 3 respectively. Similarly compound **18** gives a very clear NMR spectrum differing only in the $–CH_3$ which comes at a δ value of 2.5 ppm. The ^{1}H NMR spectrum of compound **18** is produced in figure 4.

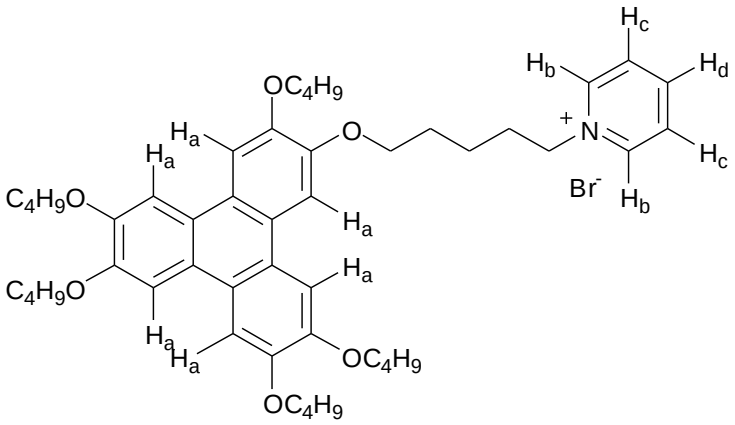

17a

Figure 5 is the reproduction of the ^{13}C NMR spectrum of compound **17a**. All the aromatic carbons and aliphatic carbons match with the expected signals. For example in the structure below all assigned carbons which are numbered are matches exactly with the spectrum.

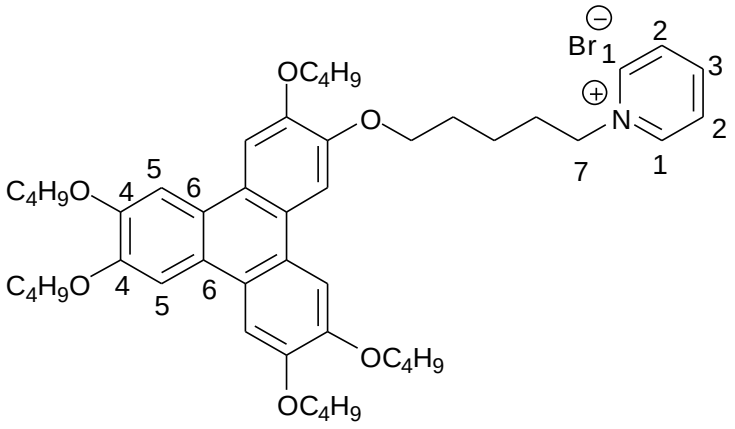

17a

1, 3, 4 carbons resonate in the region of δ 149 to δ 145 ppm. Carbon 2, 5, 6 resonate in between δ 128 to δ 107 ppm. Carbon 7 attached to pyridinium nitrogen appear with a δ value of 61.8 ppm. The –O<u>C</u>H_2 carbons resonate with δ values in between 69.7 to 69.1 ppm. Others, like –<u>C</u>H_3, -<u>C</u>H_2Me, -<u>C</u>H_2CH_2Me, -<u>C</u>$H_2CH_2CH_2N^+$-, -CH_2<u>C</u>$H_2CH_2N^+$- appear with δ values 13.9,

19.4, 31.8, 28.7, 22.9 ppm respectively. All other derivatives show similar type of NMR spectrum. The ^{13}C NMR spectrum of compound **17d** is reproduced in figure 6.

Elemental analyses of all the compounds give correct values with the errors +/- 0.4 %. All the elemental analysis data are given in the experimental section.

Figure 7 shows the IR spectrum of the compound **17a**, which shows expected aromatic and aliphatic stretching.

The UV spectra of all the samples were measured in CH_2Cl_2 and similar spectrum is obtained for all the compounds. Figure 8 represents the UV-Vis spectrum of the compound **17a**. It shows the absorption peaks at 259, 268, 278, 305, and 343 nm.

4.4.3 Thermal behavior

The thermal behaviour of all the materials was investigated by polarizing optical microscopy (POM) and differential scanning calorimetry (DSC). Transition temperatures and transition enthalpies were determined by DSC. Data obtained from the heating and cooling cycles of DSC are collected in table 2. The peak temperatures are given in °C and the numbers in the parentheses indicate the transition enthalpy (ΔH) in KJ mol^{-1}.

Compound **17a** exhibited a broad melting peak centered at about 110 °C (ΔH = 36 kJ mol^{-1}) in the first heating run of the DSC. This broad peak was composed of two non-separable peaks. During the first heating cycle, the compound did not show any definite texture, which is very common in discotic LCs, but it could be sheared easily above 95 °C indicating the presence of a liquid crystalline phase prior to the isotropic phase. The viscous phase started clearing at 104 °C which completed at 112 °C. On cooling, a well-defined texture of a columnar mesophase (figure 9) appeared at 83 °C and remained stable down to room temperature. The DSC first

cooling run showed the isotropic phase to columnar mesophase peak centered at 81 °C and no other crystallization peak was observed up to room temperature. During the second heating, the mesophase to isotropic phase transition appeared at 88 °C with a much lower heat of transition (ΔH = 3.9 kJ mol^{-1}) indicating a mesophase to isotropic transition. On second cooling, the isotropic phase to columnar mesophase peak again appeared at 81 °C.

Table 2. Phase transition temperatures (peak, ºC) and associated enthalpy changes (KJ mol^{-1}, in parentheses) of disulfide-bridged alkoxycyanibiphenyl dimers. S: solid; SS: semi solid: Col_r = columnar rectangular mesophase; I: Isotropic phase.

Compound	Heating scan	Cooling scan
17a	S-Col_r 110.0 (36) I	I 81.0 (4.4) Col_r
17b	SS 75.7 (6.3) SS 96.2 (5) Col_r 112.8 (2)--Col_r 121.2 (2.4) I	I 118.7 (2.3) Col_r 107.4 (2) Col_r
17c	SS 75.3 (6.2) SS 91.7 (4.4) Col_r 143.8 (2.9) I	I 141.1 (2.7) Col_r
17d	S 83.7 (25.5) Col_r 95.0 (5.2) I	I 92.0 (5.5) Col_r
17e	S 83.4 (3.1) SS 112.4 (36.0) I	I 100.1 (37.1) S
18	S 53.4 (29) Col_r 77.3 (1) I	I 72.7 (1) Col_r
19a	S 84.6 (32) I	I 61 (7) S
19b	S 84 (6) S 106 (37) I	I 64 (4.2) S

Compound **17b** having pentyloxy chains in the triphenylene periphery, was semi-solid at room temperature and showed three endothermic transitions prior to the isotropic transition at 121.2 °C. On cooling, the isotropic phase to mesophase transition peak appeared at 118.7 °C as well as another mesophase to mesophase transition peak at 107.4 °C. No crystallization peak up to room

temperature was observed in the DSC. However, the material was not shearable at room temperature. Probably, it vitrified and formed a stable super cooled columnar glassy phase. Under POM, the classical columnar mesophase texture appeared at about 120 °C. The texture did not show any shape change below the second transition at 107 °C but the colour of the texture did change from green to orange-red. On second heating, a very weak and broad transition occurred at about 96 °C. This could be due to the partial solidification of the material on keeping at room temperature. Therefore, the first peak in the first heating cycle at 75.7 °C was assigned to a solid to solid transition and the second peak at 96.2 °C for the melting transition. The peak at 112.8 °C was attributed to a columnar phase to columnar phase transition and the peak at 121.2 °C for the columnar phase to isotropic phase transition. The exact nature of the two mesophases could be deduced only from detailed XRD studies which have been discussed later. The DSC and POM of compound **17b** is reproduced in figure 10 and 11 respectively. Similarly, compound **17c** exhibited a solid to solid transition at 75.3 °C, a melting transition at 91.7 °C and a mesophase to isotropic phase transition at 143.8 °C. Upon cooling the columnar phase appeared (figure 12) at 141.1 °C. The DSC did not display any crystallization peak up to room temperature but the materials slowly solidified on keeping at room temperature as was evident from the melting transition at about 92 °C in the second heating cycle. Compound **17d** and **17e** were prepared to examine the effect of spacer length. Compound **17d** having butyloxy chains in the periphery and a hexamethylene spacer to connect the pyridine moiety, showed a melting transition centered at 83.7 °C (ΔH = 25.5 KJ mol^{-1}). The mesophase started clearing at 92 °C and completely changed to an isotropic phase at 102 °C. The DSC showed this broad transition with a peak at 95 °C. On cooling, POM showed the appearance of a columnar phase (figure 13) at about 100 °C. The cooling run of the DSC displayed this transition centered at 92 °C. Similar to

other samples, this material also did not exhibit any crystallization peak in the DSC. The second heating showed the melting transition at the same temperature as observed in the first heating cycle but with a smaller transition enthalpy (ΔH = 4.4 kJ mol^{-1}). This indicated the partial solidification of the material on keeping at room temperature. The columnar phase to isotropic phase transition appeared at about the same temperature and with the same transition enthalpy in the second heating run. Increasing the spacer length further, destabilized the columnar phase. Compound **17e** having butyloxy chains in the periphery and a heptamethylene spacer was found to be non-liquid crystalline. It melted at 112.4 °C to the isotropic phase and on cooling solidified at 100.1 °C. In the first heating run, it showed a solid to soft-solid transition at about 83 °C but this transition did not appear on subsequent heating. Compound **18** with 4-substituted pyridine showed a broad melting peak centered at 54 °C. The mesophase started clearing at 72 °C and completely changed to an isotropic phase at around 83 °C. The DSC showed this broad transition with a peak at 77 °C. On cooling mesophase appeared at 80 °C and remains stable down to room temperature. On second heating it does not show any melting peak. It goes directly to the isotropic phase from the columnar phase, which appears again at 80 °C on cooling. All the salts were found to be susceptible to moisture and a minor change in the thermal behaviour was observed on exposure to atmospheric moisture. Therefore, all the analyses should be performed immediately after drying the material under high vacuum at elevated temperature. Thermal behavior of **19a** and **19b** is given in section 4.4.5.

4.4.4 X-ray diffraction studies

To verify the exact nature of the mesophse of triphenylene-based pyridinium ionic liquids we performed X-ray diffraction studies. Diffraction pattern of all the compounds show a diffuse

peak in the wide angle region. It has a spacing of about 4.5 Å which corresponds to the liquid like order of the aliphatic chains. In small angle region they show several reflections which can be indexed in a simple rectangular lattice. For example compound **17a** shows six reflections with d values 38.21, 19.56, 16.02, 12.89, 10.42, 8.09 Å which can be indexed as (1,0), (2,0), (0,1), (2,1), (4,0) and (0,2) respectively. Therefore the lattice parameter a = 38.21 Å and b = 19.56 Å. The exact nature of two mesophases of compound **17b** has also been deduced from XRD studies, which confirms that both the mesophases show a columnar rectangular phase with a quite deviation of lattice parameter. All other compounds show similar behaviour in X-ray diffraction pattern. Table 3 summarizes the different d-spacings which have been indexed in a simple rectangular lattice. The X-ray diffraction pattern and one-dimensional intensity *vs*. 2θ are reproduced for compound **18** in figure 14.

Table 3: X-ray diffraction data for triphenylene-based pyridinium ionic liquid crystals

Comp	Temp. (°C)	d-spacings numbers / Å							
		d_{10}	d_{01}	d_{20}	d_{02}	d_{11}	d_{12}	d_{21}	d_{40}
17a	70	39.2	16.0	19.6	8.0			12.9	10.4
17b	115	36.6	34.1	18.6	17.2		15.6	16.4	
	90	33.3	25.0	17.5	13.2	19.7		15.2	
17c	100	41.2	35.0	20.9	17.8	25.7	16.7		
17d	80	42.4	36.4	21.5	18.3	28.3	16.2		
18	60	33.1	25.9	17.5	12.9	19.8	12.7		

4.4.5 Effect of counter ions

The replacement of counter ion used could also give an opportunity for investigating the relationship between the pyridinium moiety and its counter ion. Compound **19** was obtained from its immediate precursor **17**, as a colourless waxy solid by anion exchange from Br^- to BF_4^- using $NaBF_4$. The details of procedure have been given in experimental section. Unfortunately, tetrafluroborate counter ion destroys the liquid crystalline properties of triphenylene core, which may be due to the bulky nature of BF_4^- compare to bromide ion. In DSC they show only solid to isotropic transition on heating and on cooling from isotropic liquid to solid transition. Compound **19a** on heating melts at about 84 °C to the isotropic phase and on cooling it crystallizes at about 61 °C. Similarly, compound **19b** melts at about 106 °C to the isotropic phase and on cooling it solidifies at about 64 °C. Prior to melting transition it shows a solid to solid transition at about 84 °C. Both the compounds were characterized from there ^{1}H NMR, ^{13}C NMR, ^{19}F NMR, IR, UV spectra and elemental analysis. ^{1}H NMR and ^{13}C NMR shows almost similar spectrum with the compounds having bromide as the counter ion. ^{19}F NMR of compound **19a** is reproduced in figure 15.

4.5 Imidazolium-substituted triphenylene-based ionic liquid crystals

4.5.1 Synthesis

Imidazolium substituted triphenylenes **21** were synthesized by the route shown in scheme 2. Hexalkoxytriphenylenes **14**, monohydroxytriphenylenes **15** and ω-bromo-substituted triphenylenes **16** were prepared following literature methods [44-46] as discussed in section 4.4.1. Liquid crystalline imidazolium salts **21** were obtained by reacting the bromo-substituted compounds **16** with 1-methylimidazole or by first attaching the imidazole moiety to obtain compound **20** followed by quaternization with methyl iodide. The details of procedure have been given in experimental section.

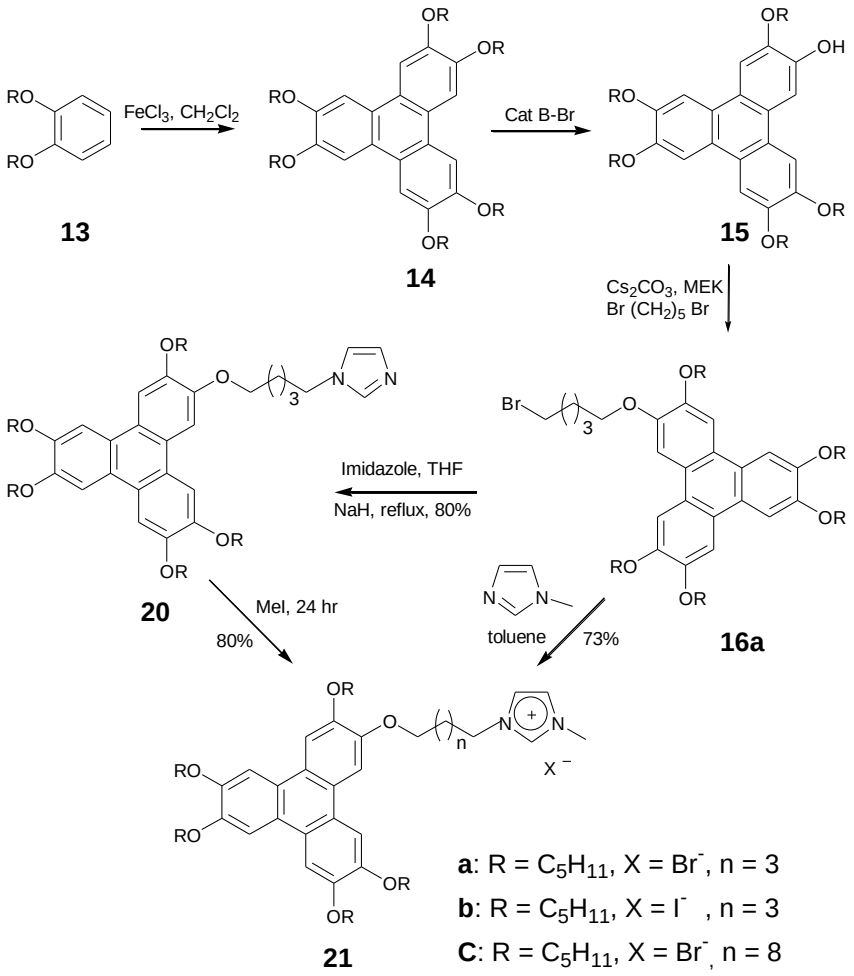

Scheme 2

4.5.2 Characterization

All the compounds were purified by repeated column chromatography followed by crystallization and characterized from their ^{1}H NMR, ^{13}C NMR, IR, UV spectra and elemental analysis. All the members of the series give similar spectra. Spectral data and elemental analysis of all the compounds were in good agreement with their structures, indicating the high purity of all the materials.

Figure 16 represents the ^{1}H NMR spectrum of compound **20**. There are four different types of aromatic protons which give rise to four signals at different δ values.

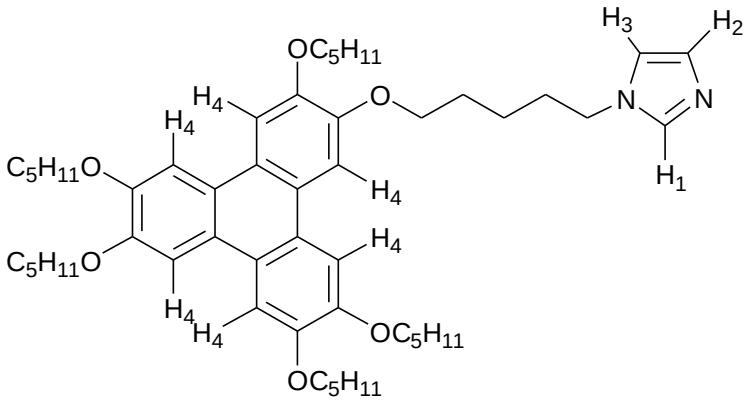

20

As can be seen from the above structure H_1 atom is flanged between two nitrogen atoms and appears as singlet at δ value of 7.49 ppm. The other two hydrogens H_2 and H_3 in the imidazolium moiety also appear as singlet at δ 7.06 and 6.93 ppm, respectively. The triphenylene hydrogens H_4 resonate at δ 7.82 ppm and appear as multiplet in the spectrum. The $-OCH_2$ and $-NCH_2$ protons resonate at δ 4.25 and 4.00, respectively. Other aliphatic protons can be clearly seen at δ 0.9-2.0 ppm in the spectrum.

Figure 17 represents the ^{1}H NMR spectrum of **21a**. There are four different types of aromatic protons which give rise to four signals at different δ values. As can be seen from the

following structure, the H_a atom is flanged between two nitrogen atoms and thus this hydrogen is more deshielded compare to all other hydrogens appears as a singlet at about δ = 10 ppm. Similarly, H_b and H_c appear as a singlet with a little difference at δ 7.20 and 7.08, respectively. Triphenylene protons (H_d) appear as a multiplet near 7.8 ppm. The $-N^+CH_2$ and $-OCH_2$ protons resonate at δ 4.34 and 4.23, respectively and appear as triplet and multiplet in NMR spectrum. The CH_3 attached to nitrogen in the imidazolium moiety appear as singlet at δ value of 4.00 ppm. Other aliphatic protons of the chain appear at 0.9-2.1 ppm. This in conjunction with the elemental analysis confirms the structure and high purity of the compound. The ^1H NMR spectrum of compound **21b** is reproduced in figure 18.

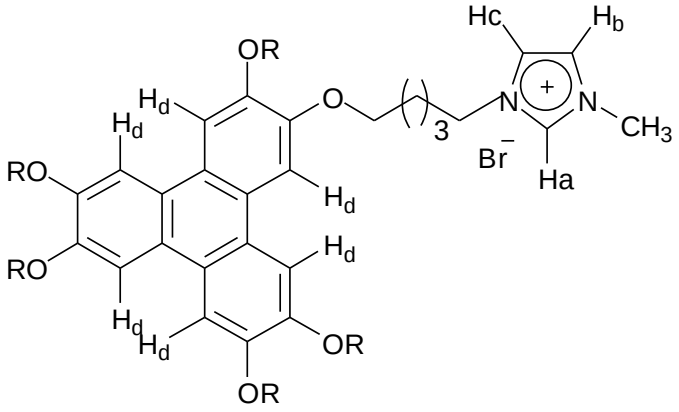

21a

The structure of imidazolium salts is further confirmed by ^{13}C NMR spectroscopy. All the aromatic carbons and aliphatic carbons match with the expected signals. For example in the structure below all assigned carbons which are numbered are matches exactly with the spectrum. All aromatic carbons (as shown by number 1) attached directly to alkoxy group resonate in the region of δ 149.2 to δ 148.7 ppm. Carbon 4 flanked between two nitrogens appear at δ value 137.6 ppm. Other two carbons 5, 6 in the imidazolium moiety and all other carbons (2, 3) in the

triphenylene moiety resonate at δ values in between 123.7 ppm to 107.3 ppm. All aliphatic carbons attached to oxygen resonate in the region of δ 69.8 to δ 69.2 ppm.

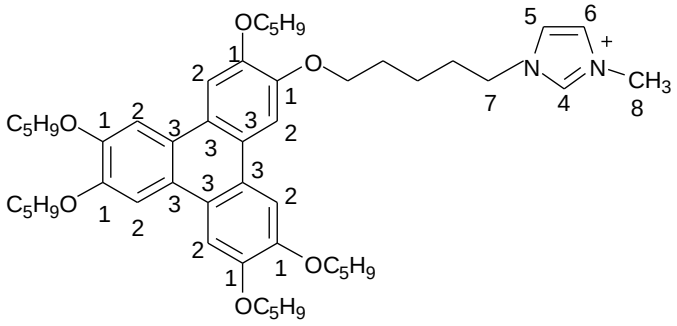

21a

Carbon 7 attached to nitrogen appear at δ value of 49.9 ppm. The $N^{+}\underline{C}H_3$ carbon appear as a singlet at δ value of 36.7 ppm. Other aliphatic carbons resonate at δ values in between 33.3 ppm to 22.5 ppm. The Methyl carbons appear at δ value of 14 ppm. The ^{13}C NMR spectrum of compound **21a** is reproduced in figure 19.

Elemental analyses of all the compounds give correct values with the errors +/- 0.4 %. All the elemental analysis data are in the experimental section.

Figure 20 shows the IR spectrum of the compound **21a**, which shows expected aromatic and aliphatic stretchings.

The UV spectra of all the samples were measured in CH_2Cl_2 and similar spectrum is obtained for all the compounds. Figure 21 represents the UV-Vis spectrum of the compound **21a**. It shows the absorption peaks at 258, 269, 278, 305, and 344 nm.

4.5.3 Thermal behaviour

The thermal behaviour of all the materials was investigated by polarizing optical microscopy (POM) and differential scanning calorimetry (DSC). Transition temperatures and transition

enthalpies were determined by DSC. Data obtained from the heating and cooling cycles of DSC are collected in table 4. The peak temperatures are given in °C and the numbers in the parentheses indicate the transition enthalpy (ΔH) in KJ mol^{-1}.

Table 4. Phase transition temperatures (peak temperature/°C) and associated enthalpy changes (KJ mol^{-1} in parentheses) of novel triphenylene-substituted imidazolium salts. S = semi-solid, Col_r = columnar rectangular phase, I = isotropic.

Compound	Heating scan	Cooling scan
20	Cr 50 (35) I	-
21a	S 67 (24) Col_r 101 (2.3) I	I 98 (2.3) Col_r 38 (21) S
21b	S 64 (21) Col_r 83 (2.1) I	I 79 (2.0) Col_r 44 (27) S
21c	S 59 (28) Col_r 96 (2.6) I	I 93 (2.4) Col_r 42 (22) S

It is interesting to note that the non-ionic imidazole-substituted triphenylene derivative **20** was found to be non-liquid crystalline. The crystalline compound **20** melts at 50 °C to the isotropic phase. On cooling it does not crystallize upto room temperature. The DSC of compound **20** is reproduced in figures 22. Compound **21a** exhibited a broad melting peak centered at about 67 °C and a mesophase to isotropic peak centered at about 101 °C in the first heating run of the DSC. On cooling, the isotropic phase to mesophase peak appeared at 98 °C which solidified at 38 °C. The photomicrograph of **21a** is reproduced in figure 23. Compound **22b** showed the melting transition at 64 °C and the isotropic phase transition at 83 °C in the first heating run. On cooling, the mesophase appeared (as shown in figure 24) at 79 °C and the crystallization peak appeared at 44 °C. The DSC traces obtained on heating and cooling runs for **22b** are shown in Figure 25. Compound **21c**

exhibited a broad melting peak at about 59 °C. The mesophase started clearing at about 90 °C and completely changed to an isotropic phase at 100 °C. The DSC showed this broad transition with a peak at 96 °C. On cooling, POM showed the appearance of columnar phase at about 96 °C. The cooling run of DSC displayed this transition centered at 93 °C and the crytallisation peak appeared at 42 °C. All imidazolium salts were found to be hygroscopic in nature and a minor increase in the isotropic temperature was observed on exposure to atmospheric pressure.

4.5.4 X-ray diffraction studies

To verify the exact nature of the mesophases we performed X-ray diffraction studies, which is similar to what we get with pyridinium ionic salts. All compounds show a columnar mesophase which can be indexed in a simple rectangular lattice. For example compound **21a** showed several reflections in small angle region which has been indexed as (1, 0), (0, 1), (2, 0), (0, 2), (1, 2), (2, 1), (1, 1), (3, 0). The lattice parameter calculated from the diffraction pattern with a = 57.55 mm, b = 43.98 mm. The X-ray diffraction pattern is reproduced in figure 26. Diffraction pattern of all the compounds show a diffuse peak in the wide angle region. It has a spacing of about 0.45 nm which corresponds to the liquid like order of the aliphatic chains.

4.6 Conclusion

In conclusion, we have prepared several pyridinium and imidazolium ionic salts connected with well-known triphenylene-based discotic liquid crystals. Increasing the number of carbon atoms on the peripheral chains of the triphenylene core stabilized the columnar phase while increasing the spacer length connecting the triphenylene unit with the pyridine moiety destabilized the mesophase. The variation of counter ion from Br^- to BF_4^- destroys the liquid crystalline property

of these salts. These are the first known thermotropic ionic liquid crystals based on triphenylene. These salts are not only important for a new possibility of organic molten salts in materials science, but also contribute to the development of novel anisotropic soft materials for directional ion conductivity and charge transport.

4.7 Experimental

4.7.1 General information

General experimental conditions have been described in chapter 2.

4.7.2 Synthesis of prridinium-substituted triphenylene-based ionic liquid crystals

The synthesis of **14**, **15**, and **16** has been described elsewhere [45-47, 47].

Synthesis of 17a: In a round bottom flask, 0.1 g of compound **16a** was dissolved in 2.5 ml of toluene. To this, 2 ml of pyridine was added and the reaction mixture was heated at 80 °C for 8 hours under nitrogen with stirring. The solvent and excess of pyridine were removed under vacuum and the residue was recrystallized twice from dry diethyl ether to afford the quaternized product **17a** (90.5 mg, 83 %).

Compound **17a**: **^{1}H NMR** (400 MHz, $CDCl_3$): δ 9.46 (d, *J* = 5.7 Hz, 2H), 8.31 (t, *J* = 7.8 Hz, 1H), 7.95 (t, *J* = 7.0 Hz, 2H), 7.82 (m, 6H), 5.07 (t, *J* = 7.4 Hz, 2H), 4.29 (m, 12H), 1.40-2.26 (m, 26H), 0.97 (m, 15H).

^{13}C NMR (100 MHz, $CDCl_3$ all the derivatives **17a-17e** show similar spectrum): δ 149.1, 148.6, 144.9, 144.7, 128.0, 123.6, 123.4, 123.3, 107.3, 69.7, 69.6, 69.1, 61.6, 31.8, 28.7, 22.9, 19.4 13.9.

IR (KBr, all the derivatives **17a-17e** show similar spectrum): ν_{max} 2930, 2856, 1618, 1518, 1435, 1389, 1261, 1173, 1053, 1033, 835 cm^{-1}.

UV-Vis ($CHCl_3$, all the derivatives **17a-17e** show similar spectrum): λ_{max} 305, 344, 359 nm. **Elemental analysis**: calculated for $C_{48}H_{66}O_6NBr$, C 69.21, H 7.93, N 1.68 %; found C 69.12, H 8.01, N 1.62 %.

Compound **17b**: **^{1}H NMR** (400 MHz, $CDCl_3$): δ 9.45 (d, *J* = 5.7 Hz, 2H), 8.30 (t, *J* = 7.8 Hz, 1H), 7.95 (t, *J* = 7.0 Hz, 2H), 7.82 (m, 6H), 5.07 (t, *J* = 7.4 Hz, 2H), 4.29 (m, 12H), 1.40-2.28 (m, 36H), 0.98 (m, 15H).

Elemental analysis: calculated for $C_{53}H_{76}O_6NBr$, C 70.5, H 8.42, N 1.55 %; found C 70.0, H 8.52, N 1.43 %.

Compound **17c**: **^{1}H NMR** (400 MHz, $CDCl_3$): δ 9.45 (d, *J* = 5.7 Hz, 2H), 8.30 (t, *J* = 7.8 Hz, 1H), 7.95 (t, *J* = 7.0 Hz, 2H), 7.82 (m, 6H), 5.07 (t, *J* = 7.4 Hz, 2H), 4.29 (m, 12H), 1.40-2.28 (m, 46H), 0.98 (m, 15H).

Elemental analysis: calculated for $C_{58}H_{86}O_6NBr$, C 71.6, H 8.84, N 1.44 %; found C 71.0, H 8.57, N 1.40 %.

Compound **17d**: **^{1}H NMR** (400 MHz, $CDCl_3$): δ 9.35 (d, *J* = 5.7 Hz, 2H), 8.25 (t, *J* = 7.8 Hz, 1H), 7.95 (t, *J* = 7.0 Hz, 2H), 7.82 (m, 6H), 5.07 (t, *J* = 7.4 Hz, 2H), 4.29 (m, 12H), 1.4-2.2 (m, 28H), 0.98 (m, 15H).

Elemental analysis: calculated for $C_{49}H_{68}O_6NBr$, C 69.5, H 8.03, N 1.65 %; found C 69.1, H 8.11, N 1.60 %.

Compound **17e**: **^{1}H NMR** (400 MHz, $CDCl_3$): δ 9.35 (d, *J* = 5.7 Hz, 2H), 8.25 (t, *J* = 7.8 Hz, 1H), 7.95 (t, *J* = 7.0 Hz, 2H), 7.82 (m, 6H), 5.07 (t, *J* = 7.4 Hz, 2H), 4.29 (m, 12H), 1.4-2.2 (m, 30H), 0.98 (m, 15H).

Elemental analysis: calculated for $C_{50}H_{70}O_6NBr$, C 69.7, H 8.14, N 1.62 %; found C 69.5, H 8.10, N 2.20 %.

Compound **18**: **^{1}H NMR** (400 MHz, $CDCl_3$): δ 9.15 (d, *J* = 5.7 Hz, 2H), 7.82 (m, 6H), 7.70 (d, *J* = 5.7 Hz, 2H), 4.95 (t, *J* = 7.4 Hz, 2H), 4.29 (m, 12H), 2.5 (s, 1H), 1.4-2.2 (m, 36H), 0.95 (m, 15H).

Elemental analysis: calculated for $C_{54}H_{79}O_6NBr$, C 70.7, H 8.61, N 1.52 %; found C 70.4, H 7.49, N 2.00 %.

Compound **19a**: **^{1}H NMR** (400 MHz, $CDCl_3$): δ 9.46 (d, *J* = 5.7 Hz, 2H), 8.31 (t, *J* = 7.8 Hz, 1H), 7.95 (t, *J* = 7.0 Hz, 2H), 7.82 (m, 6H), 5.07 (t, *J* = 7.4 Hz, 2H), 4.29 (m, 12H), 1.40-2.26 (m, 26H), 0.97 (m, 15H).

^{19}F NMR (400 MHz, $CDCl_3$): - 151.7- 151.9 (m).

Elemental analysis: calculated for $C_{48}H_{66}O_6NBF_4$, C 68.6, H 7.87, N 1.67 %; found C 68.5, H 8.10, N 1.50 %.

Compound **19b**: **^{1}H NMR** (400 MHz, $CDCl_3$): δ 9.35 (d, *J* = 5.7 Hz, 2H), 8.25 (t, *J* = 7.8 Hz, 1H), 7.95 (t, *J* = 7.0 Hz, 2H), 7.82 (m, 6H), 5.07 (t, *J* = 7.4 Hz, 2H), 4.29 (m, 12H), 1.4-2.2 (m, 28H), 0.98 (m, 15H).

Elemental analysis: calculated for $C_{49}H_{68}O_6NBF_4$, C 68.9, H 7.97, N 1.64 %; found C 68.2, H 7.95, N 1.20 %.

4.7.3 Synthesis of imidazolium-substituted triphenylene-based ionic liquid crystals

Synthesis of 20: A DMF solution of imidazole (50 mg, 0.735 mmol) in a round-bottomed flask (50 ml) equipped with a stirring bar was deaerated under reduced pressure, and the flask was filled with argon. The deaeration was repeated three times to remove oxygen in the flask, thoroughly. The flask was kept in an ice-bath to maintain the temperature of about 0 °C inside. After that 19 mg of NaH (0.8 mmol) was added slowly into the reaction mixture. Then 300 mg of

triphenylene bromide **16a** (0.4 mmol) was added and the resulting mixture was heated at 70 °C for 2 h with vigorous stirring. After the reaction is over, the mixture was poured into a mixture of ethyl acetate (EtOAc) and water (50 ml). The organic phase was separated; the aqueous phase was extracted with EtOAc three times. The combined organic extracts were washed with water and saturated NaCl solution respectively. The resulting organic phase was dried over anhydrous sodium sulfate and concentrated under reduced pressure. The residue was purified through a small silica column (3-5 % ethyl acetate) to give pure product (20 mg, 68 %).

Compound **20**: **^{1}H NMR** (400 MHz, $CDCl_3$): δ 7.83 (6H, m) 7.5 (1H, s) 7.07 (s, 1H), 6.93 (s, 1H), 4.24 (m, 12 H), 4.00 (t, 3H), 1.4-2.0 (m, 35H), .99 (m, 15H).

Elemental analysis: calculated for $C_{51}H_{74}O_6N_2$, C 75.5, H 9.10, N 3.07 %; found C 75.1, H 9.10, N 3.22 %.

Synthesis of 21a: A toluene (2 ml) solution of compound **16a** (0.1 g, 0.12 mmol) and distilled 1-methylimidazole (3 ml, excess) in a round bottomed flask equipped with a stirring bar was heated at 80 °C for 8 h with vigorous stirring. The solvent was removed in vaccuo, and the residue was recrystalised from dry diehylether three times to give 0.99g (86 %).

Synthesis of 21b: Compound **21b** having I^- as a counter ion was obtained by reacting **20** (0.1 g, 0.12 mmol) with excess of methyl iodide with vigorous stirring at room temperature for 24 h. The compound was then recrystallised from hexane three times to give the pure product (0.90 g, 77 %).

Compound **21a**: **^{1}H NMR** (400 MHz, $CDCl_3$): δ 10.85 (s, 1H), 7.82 (m, 6H), 7.21 (s, 1H), 7.10 (s, 1H), 4.40 (t, J = 7.2 Hz, 2H), 4.23 (m, 12H), 4.00 (s, 3H), 1.43-2.16 (m, 36H), 0.95 (m, 15H).

^{13}C NMR (100 MHz, $CDCl_3$): δ 149.2, 149.1, 148.8, 148.7, 137.7, 123.8, 123.7, 123.6, 123.5, 123.2, 121.8, 107.6, 107.4, 70.0, 69.8, 69.7, 69.2, 50.0, 36.7, 29.9, 29.2, 28.7, 28.4, 23.1, 22.6, 14.1.

IR (KBr): ν_{max} 2953, 2930, 2856, 1616, 1518, 1437, 1389, 1261, 1173, 1053, 1032, 835 cm^{-1}.

UV-Vis ($CHCl_3$): λ_{max} 304, 344, 360 nm.

Elemental analysis: calculated for $C_{52}H_{77}O_6N_2Br$, C 68.9, H 8.50, N 3.1 %; found C 68.4, H 8.57, N 3.62 %.

Compound **21b**: **^{1}H NMR** (400 MHz, $CDCl_3$): δ 10.03 (s, 1H), 7.82 (m, 6H), 7.20 (s, 1H), 7.08 (s, 1H), 4.34 (t, *J* = 7.2 Hz, 2H), 4.23 (m, 12H), 4.00 (s, 3H), 1.43-2.16 (m, 36H), 0.95 (m, 15H).

^{13}C NMR (100 MHz, $CDCl_3$): δ 149.2, 149.1, 148.8, 148.7, 137.7, 123.8, 123.7, 123.6, 123.5, 123.2, 121.8, 107.6, 107.4, 70.0, 69.8, 69.7, 69.2, 50.0, 36.7, 29.9, 29.2, 28.7, 28.4, 23.1, 22.6, 14.1.

IR (KBr): ν_{max} 2953, 2930, 2856, 1616, 1518, 1437, 1389, 1261, 1173, 1053, 1032, 835 cm^{-1}.

UV-Vis ($CHCl_3$): λ_{max} 304, 344, 360 nm.

Elemental analysis: calculated for $C_{52}H_{77}O_6N_2I$, C 65.5, H 8.1, N 2.9 %; found C 65.7, H 8.1, N 2.7 %.

Compound **21c**: **^{1}H NMR** (400 MHz, $CDCl_3$): δ 10.73 (s, 1H), 7.82 (m, 6H), 7.20 (s, 1H), 7.08 (s, 1H), 4.34 (t, *J* = 7.2 Hz, 2H), 4.23 (m, 12H), 4.00 (s, 3H), 1.43-2.16 (m, 46H), 0.95 (m, 15H).

Elemental analysis: calculated for $C_{57}H_{87}O_6N_2Br$, C 70.1, H 8.98, N 2.87 %; found C 70.5, H 8.90, N 2.7 %.

References

[1] A. Getsis, A-Verena. Mudring, *Zeitschrift fur anorgnische und allgemeine Chemie*, **632**, 2106 (2006).

[2] T. Welton, *Chem Rev*., **99**, 2071 (1999).

[3] R. Sheldon, *Chem Commun*., 2399 (2001).

[4] K. R. Sheldon, *J. Chem. Technol. Biotecnol*., **68**, 351 (1997).

[5] M. J. Earle, K. R. Sheldon, *Pure Appl. Chem*., **72**, 1391 (2000).

[6] J. Dupont, R. F. de Souza, P. A. Z. Saurez, *Chem Rev*., **102**, 3667 (2002).

[7] P. Wasserscheid, W. Keim, *Angew. Chem., Int. Ed*., **39**, 3772 (2000).

[8] P. Wasserscheid, T. Welton, (Eds.), *Ionic Liquids in Synthesis*, Wiley-VCH, Weinheim, (2002).

[9] H. Ohno., (Eds.), *Electrochemical Aspects of Ionic Liquids*, Wiley, New York, (2005)

[10] C. Tschierske, *Curr. Opin. Colloid Interface Sci.*, **7**, 355 (2002).

[11] (a) R. G. Weiss, *Tetrahedron*, **44**, 3413 (1988). (b) H. Kansui, S. Hiraoka, T. Kunieda, *J. Am. Chem. Soc.*, **118**, 5346 (1996).

[12] (a) N. Yamanaka, R. Kawano, W. Kubo, T. Kitamura, Y. Wada, M. Watanabe, S. Yanagida, *Chem. Commun*., 740 (2005). (b) W. A. Henderson, S. Passerini, *Chem. Mater.*, **16**, 2881 (2004) and references therein.

[13] A. Skoulios, *Adv. Coll. Interface Sci.*, **1**, 79 (1967).

[14] D. W. Bruce, D. A. Dunmur, E. Lalinde, P. M. Maitlis, P. Styring, *Nature*, **323**, 7 91 (1986).

[15] M. Marcos, M. B. Ros, J. L. Serrano, M. A. Esteruelas, E. Sola, L. A. Oro, J. Barbera, *Chem. Mater*., **2**, 748 (1990).

[16] E. Bravo-Grimaldo, D. Navarro-Rodriguez, A. Skoulios, D. Guillon, *Liq. Cryst.*, **20**, 323 (1996).

[17] H. Bernhardt, W. Weissflog, H. Kresse, *Liq. Cryst.*, **24**, 895 (1998).

[18] C. M. Gordon, J. D. Holbrey, A. R. Kennedy, K. R. Seddon, *J. Mater. Chem.*, **8**, 2627 (1998).

[19] D. Tsiourvas, D. Kardassi, C. M. Paleos, A. Skoulios, *Liq. Cryst.*, **27**, 1213 (1998).

[20] J. D. Holbrey, K. R. Seddon, *J. Chem. Soc. Dalton Trans.*, 2133 (1999).

[21] L. Cui, V. Sapagovas, G. Lattermann, *Liq. Cryst.*, 29, 1121 (2002).

[22] J. De Roche, C. M. Gordon, C. T. Imrie, M. D. Ingram, A. R. Kennedy, F. L. Celso, A. Triolo, *Chem. Mater.*, **15**, 3089 (2003).

[23] P. K. Bhowmik, H. Han, I. K. Nedeltchev, J. J. Cebe, *Mol. Cryst. Liq. Cryst.*, **419**, 27 (2004).

[24] D. Haristoy, D. Tsiourvas, *Liq. Cryst.*, **31**, 697 (2004).

[25] H. Yoshizawa, Mihara, N. Koide, *Mol. Cryst. Liq. Cryst*., **423**, 61 (2004).

[26] K. M. Lee, C. K. Lee, I. J. B. Lin, *Chem. Commun*., 899 (1997).

[27] K. M. Lee, Y. T. Lee, I. J. B. Lin, *J. Mater. Chem.*, **13**, 1079 (2003).

[28] M. Yoshio, T. Kato, T. Mukai, M. Yoshizawa, H. Ohno, *Mol. Cryst. Liq. Cryst.*, **413**, 99 (2004).

[29] M. Yoshio, T. Mukai, K. Kanie, M. Yoshizawa, H. Ohno, T. Kato, *Adv. Mater*., **14**, 351 (2002).

[30] K. Binnemans, *Chem Rev*., **105**, 4148 (2005).

[31] R. Keller-Griffith, H. Ringsdorf, A. Vierengel, *Colloid Poly. Sci.*, **264**, 924 (1986).

[32] M. Veber, G. Berruyer, *Liq. Cryst.*, **27**, 671 (2000).

[33] C. F. van Nostrum, R. J. M. Nolte, *Chem. Commun*., 2385 (1996).

[34] V. Percec, G. Johansson, J. Heck, G. Ungar, S. V. Batty, *J. Chem. Soc., Perkin. Trans., 1* 1411 (1993).

[35] M. Yoshio, T. Mukai, H. Ohno, T. Kato, *J. Am. Chem. Soc.*, **126**, 994 (2004).

[37] J. Kadam, C. F. J. Faul, U. Scherf, *Chem. Mater.*, **16**, 3867 (2004).

[38] A. Kraft, A. Reichert, R. Kleppinger, *Chem Commun*., 1015 (2000).

[39] J. Motoyanagi, T. Fukushima, T. Aida, *Chem. Commun*., **11**, 101 (2005).

[40] C. Destrade, N. H. Tinh, H. Gasparoux, J. Malthete, A. M. Levelut, *Mol. Cryst. Liq. Cryst*., **71**, 111 (1981).

[41] S. Kumar, *Chem. Soc. Rev*., **35**, 83 (2006).

[42] T. Kato, *Science*, **295**, 2414 (2002).

[43] S. Kumar, *Liq. Cryst*., **32**, 1089 (2005).

[44] S. Kumar, M. Manickam, *Chem Commun*., 1615 (1997).

[45] S. Kumar, M. Manickam, *Synthesis*, 1119 (1998).

[46] S. Kumar, J. J. Naidu, S. K. Varshney, *Mol. Cryst. Liq. Cryst*., **411**, 355 (2004).

[47] N. Boden, R. J. Bushby, P. S. Martin, *Langmuir*, **15**, 3790 (1999).

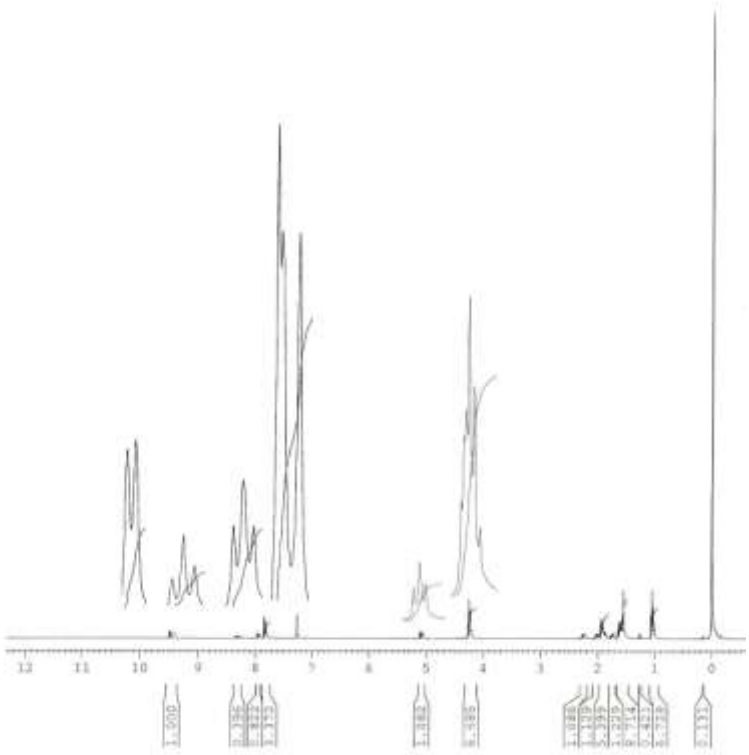

Figure 1. [1]H NMR spectrum of the compound **17a**.

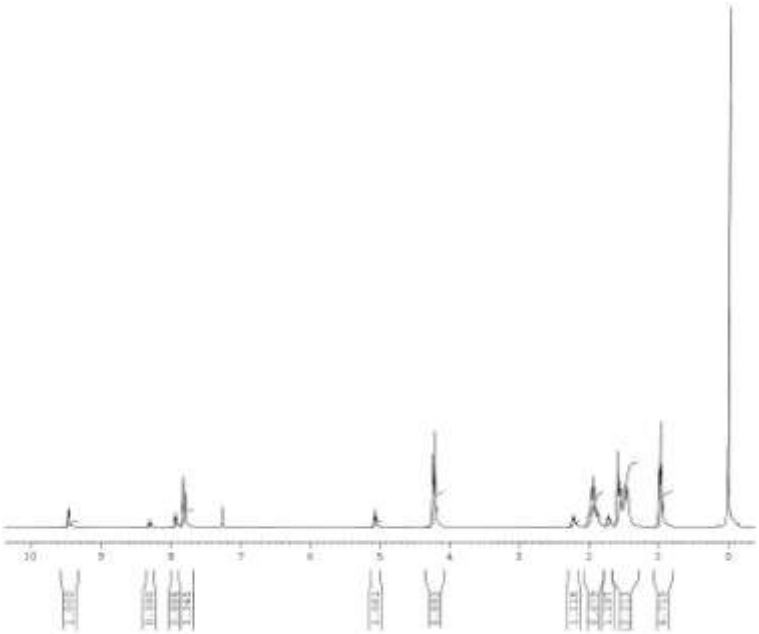

Figure 2. [1]H NMR spectrum of the compound **17b**.

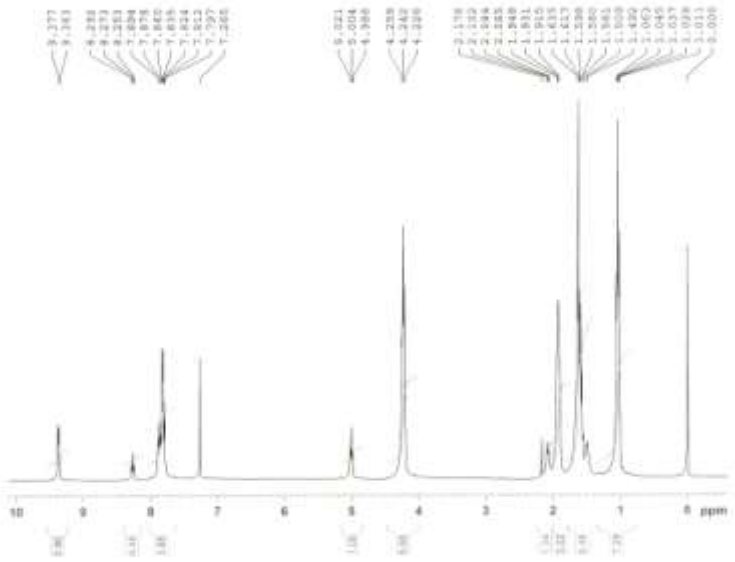

Figure 3. ^{1}H NMR spectrum of the compound **17d**.

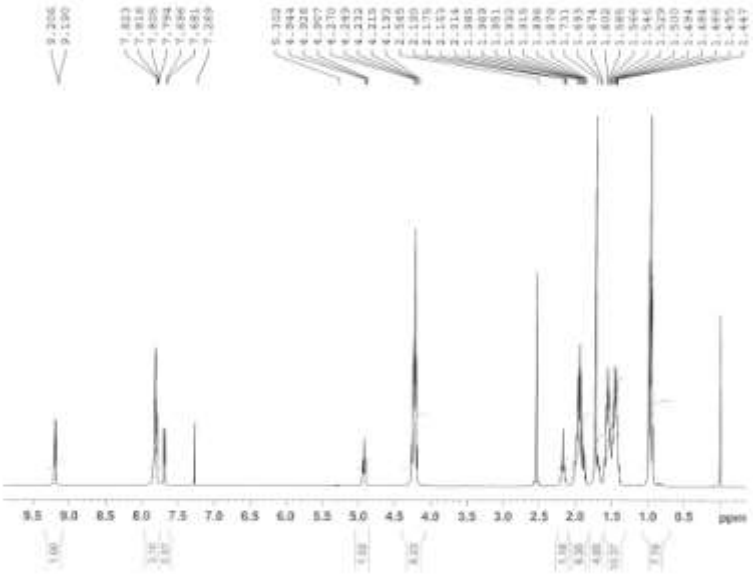

Figure 4. ^{1}H NMR spectrum of the compound **18**.

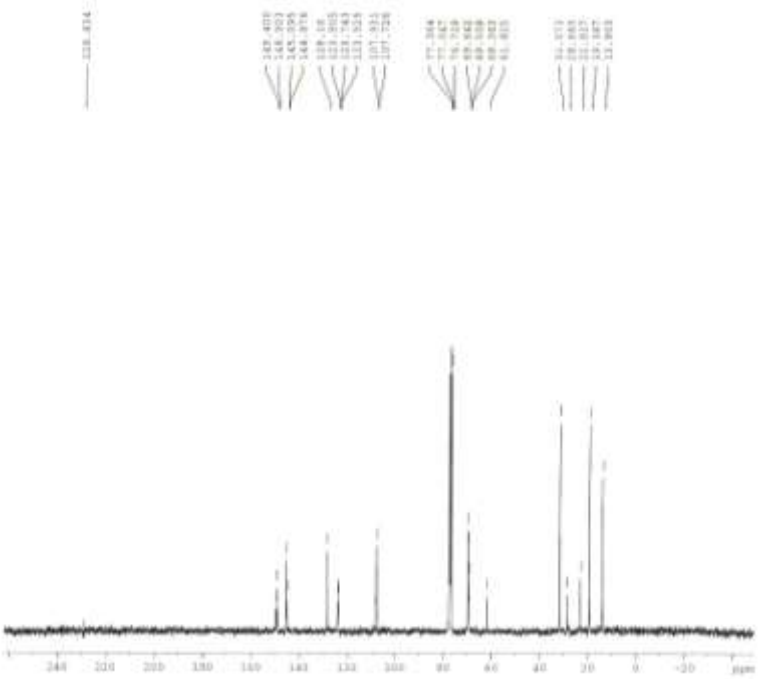

Figure 5. ^{13}C NMR spectrum of the compound **17a**.

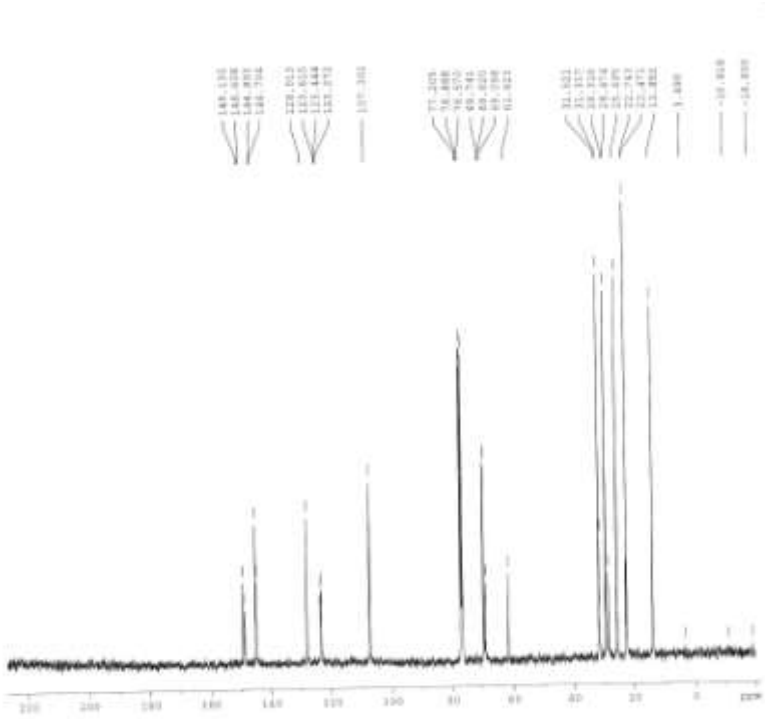

Figure 6. ^{13}C NMR spectrum of the compound **17d**.

Figure 7. IR spectrum of the compound **17a**.

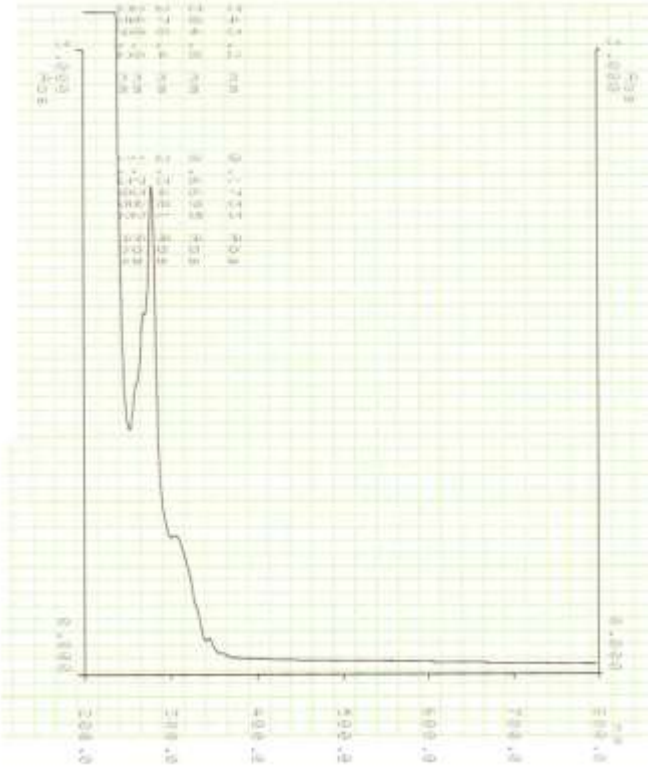

Figure 8. UV spectrum of the compound **17a**.

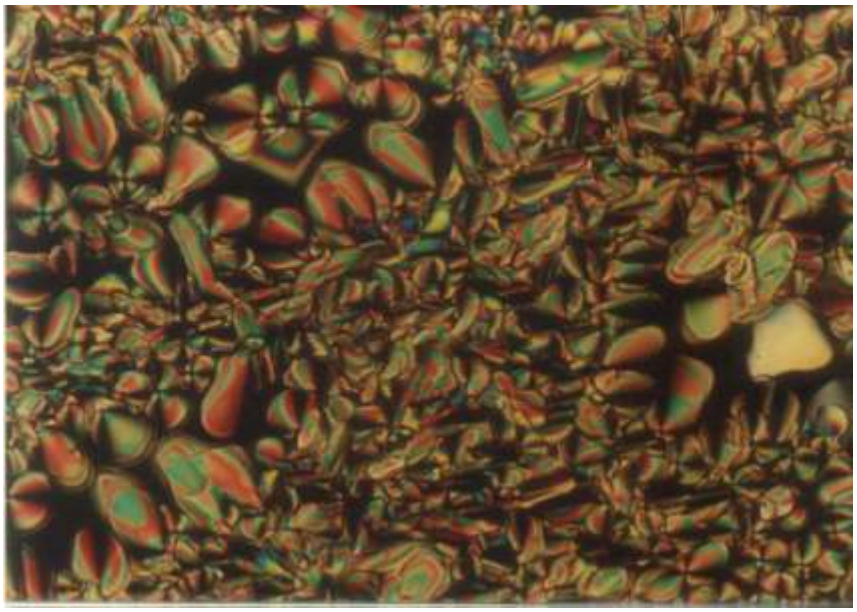

Figure 9. Optical photomicrograph of **17a** obtained with a polarizing microscope on cooling from the isotropic liquid at 78 °C (crossed polarizers, magnification X 200).

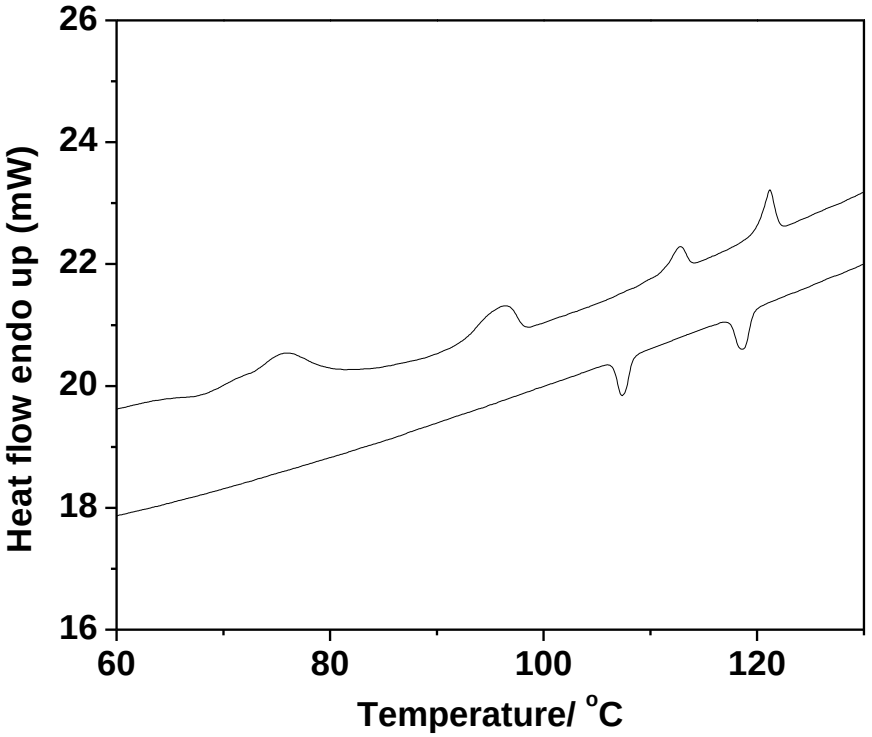

Figure 10. DSC traces for compound **17b** on heating and cooling (scan rate 5 °C/min).

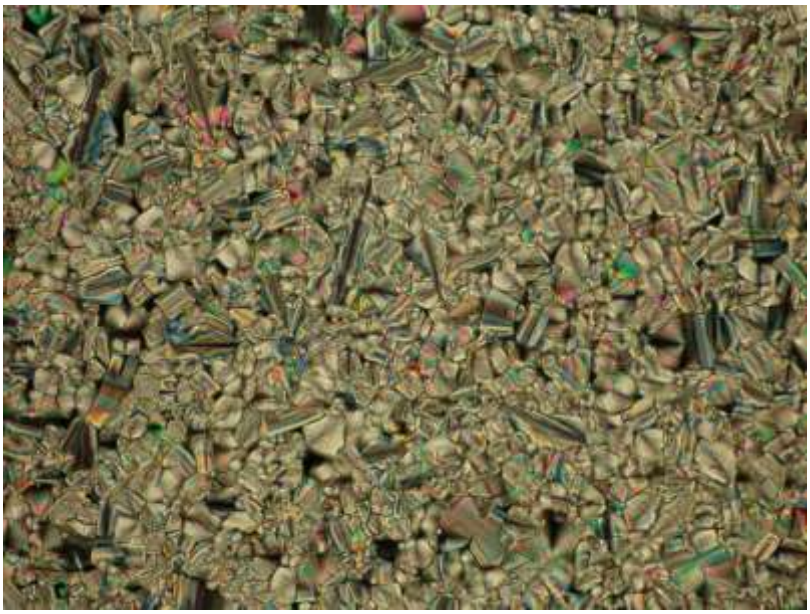

Figure 11. Optical photomicrograph of **17b** obtained with a polarizing microscope on cooling from the isotropic liquid at 100 °C (crossed polarizers, magnification X 200).

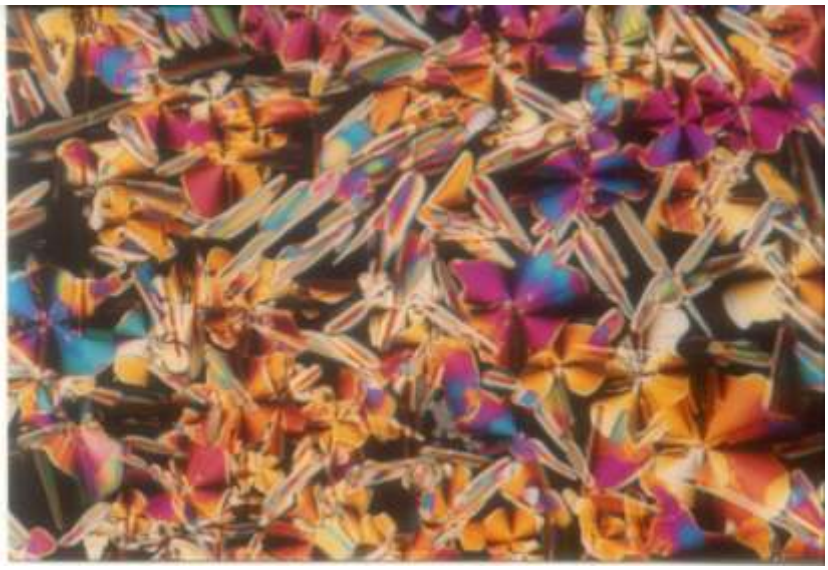

Figure 12. Optical photomicrograph of **17c** obtained with a polarizing microscope on cooling from the isotropic liquid at 130 °C (crossed polarizers, magnification X 200).

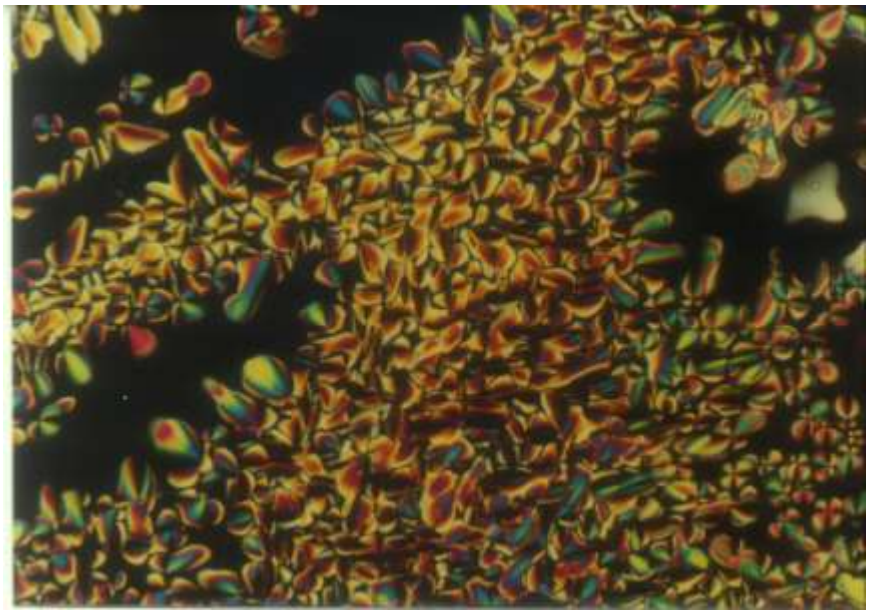

Figure 13. Optical photomicrograph of **17d** obtained with a polarizing microscope on cooling from the isotropic liquid at 85 °C (crossed polarizers, magnification X 200).

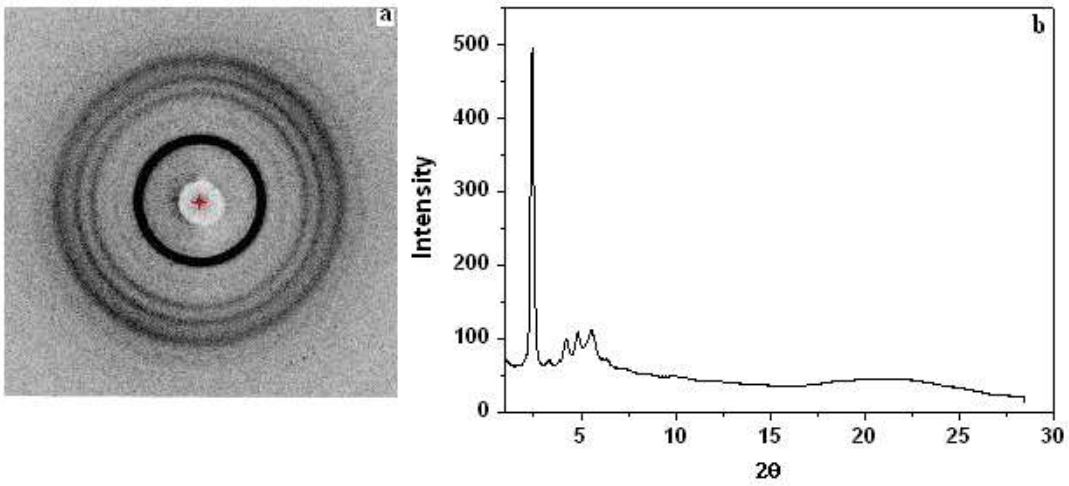

Figure 14. (a) X-ray diffraction pattern and (b) one-dimensional intensity *vs*. 2θ (deg.) for compound **18** at room temperature.

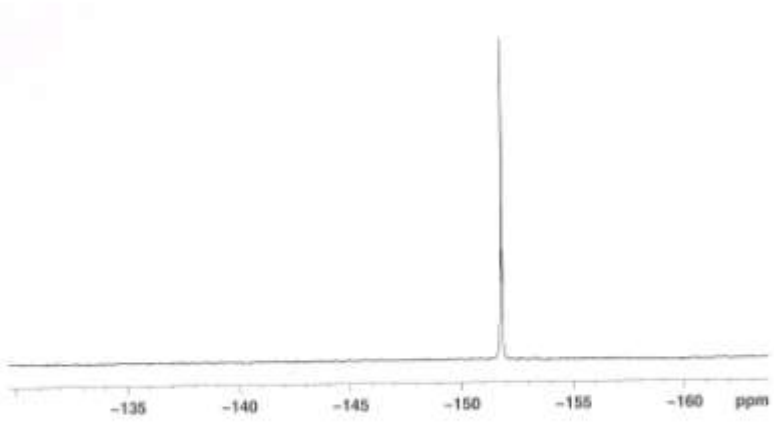

Figure 15. ^{19}F spectrum of the compound **19a**.

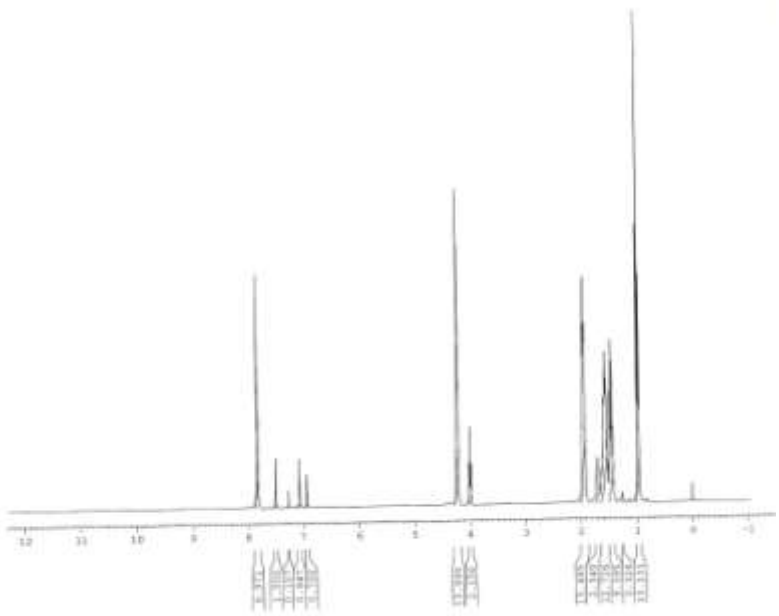

Figure 16. ^{1}H NMR spectrum of the compound **20**.

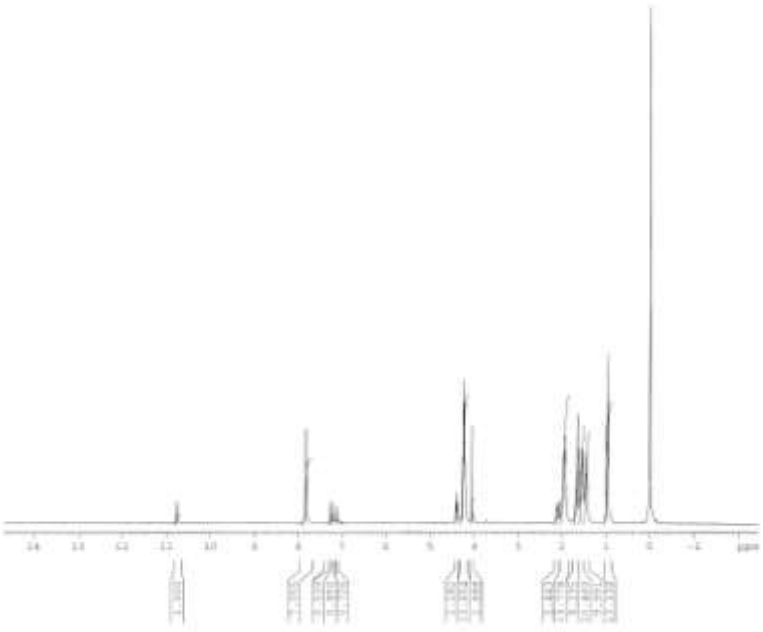

Figure 17. ^{1}H NMR spectrum of the compound **21a**.

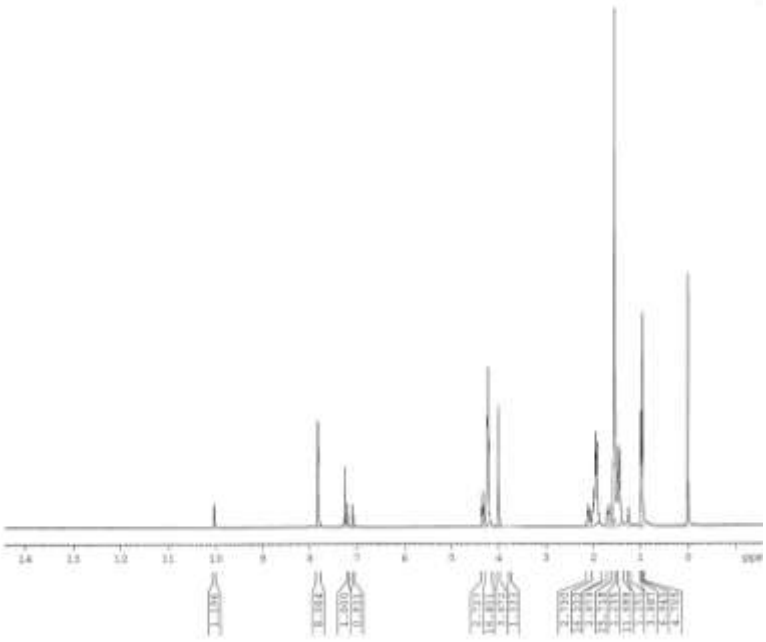

Figure 18. ^{1}H NMR spectrum of the compound **21b**.

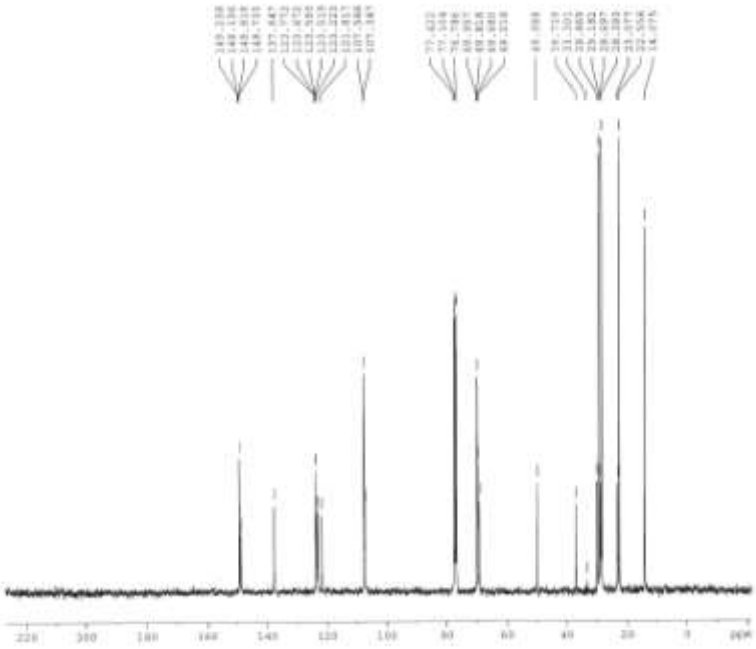

Figure 19. ^{13}C NMR spectrum of the compound **21a**.

Figure 20. IR spectrum of the compound **21a**.

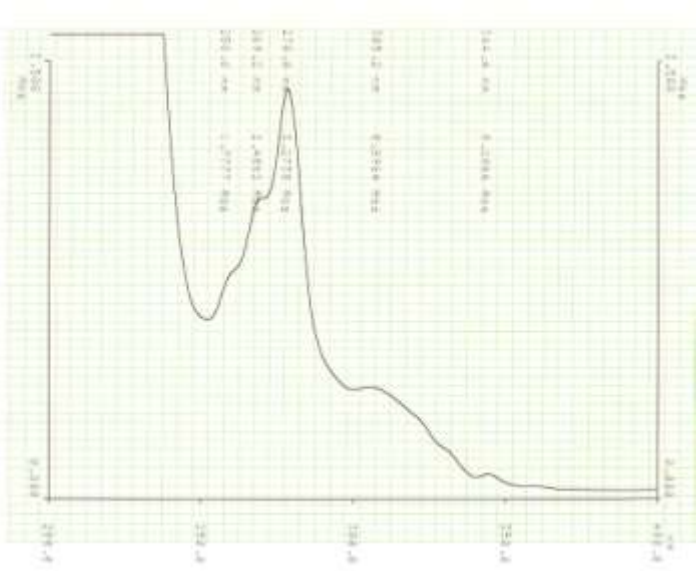

Figure 21. UV spectrum of the compound **21a**.

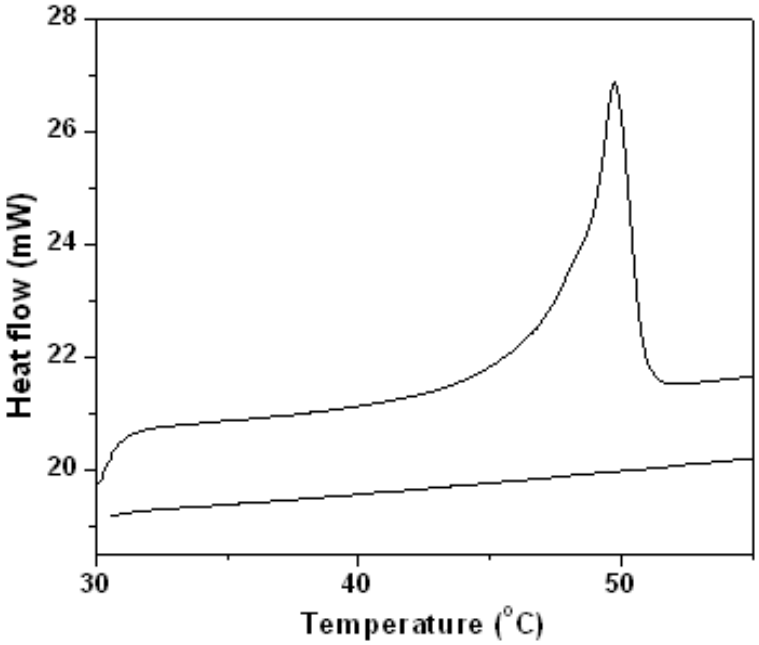

Figure 22. DSC traces for compound **20** on heating and cooling (Scan rate 5 °C/min).

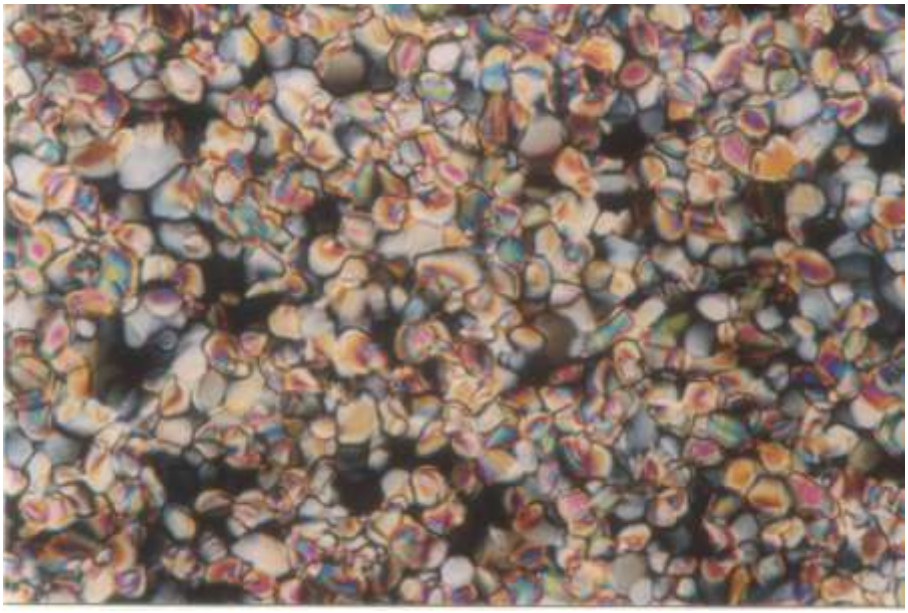

Figure 23. Optical photomicrograph of **21a** obtained with a polarizing microscope on cooling from the isotropic liquid at 70 °C (crossed polarizers, magnification X 200).

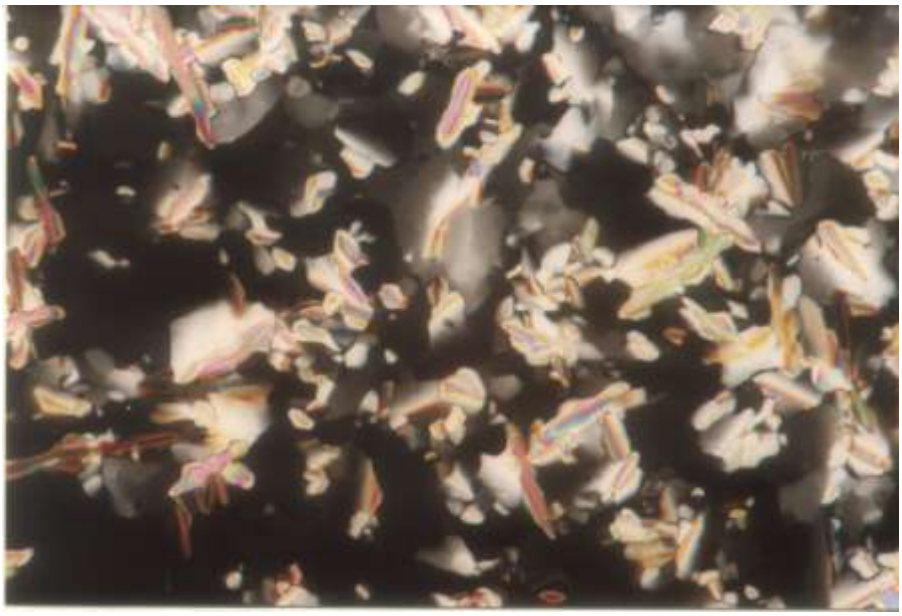

Figure 24. Optical photomicrograph of **21b** obtained with a polarizing microscope on cooling from the isotropic liquid at 70 °C (crossed polarizers, magnification X 200).

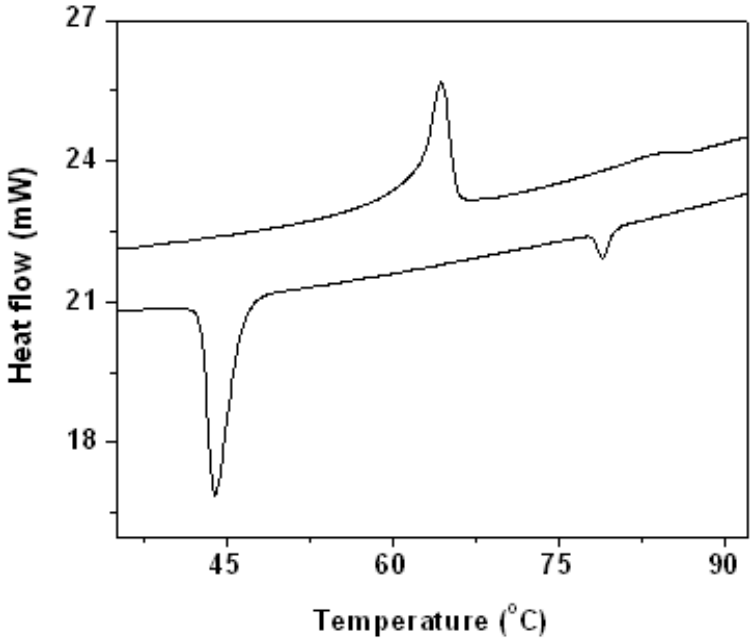

Figure 25. DSC traces of **21b** on heating and cooling (scan rate 5 °C/min).

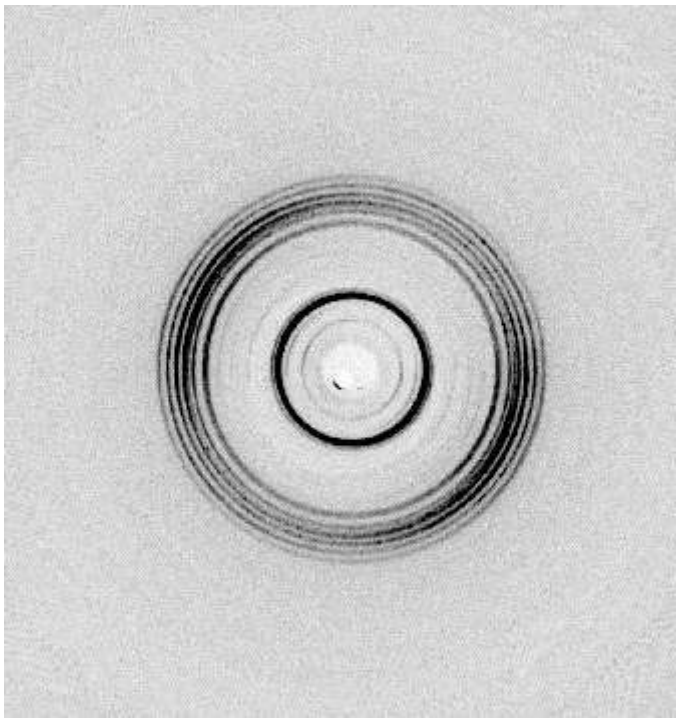

Figure 26. X-ray diffraction pattern obtained for compound **21a** at 70 °C.